UNIVERSIDAD TÉCNICA FEDERICO SANTA MARÍA

DEPARTMENT OF CHEMICAL AND ENVIRONMENTAL ENGINEERING

VALPARAISO, CHILE

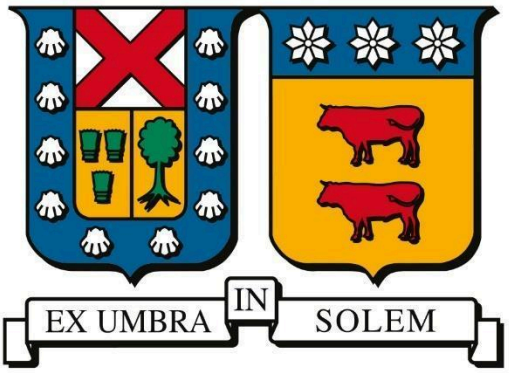

"Experimental Evaluation and Modeling of Leaching Kinetics and Fine Particle Challenges in Sodium Chloride and Sulfuric Acid Solutions for Lithium-Ion Battery Recycling Plant Design"

Ruvi Jade Cubarol

THESIS TO OBTAIN THE DEGREE OF MASTER OF SCIENCE IN CHEMICAL ENGINEERING

Main supervisor: Claudio Acuña Pérez

Co-supervisor: Luis Vinnett Peralta

External supervisor: Julio Valenzuela

Joint Master Erasmus Mundus

June 2024

VALIDATION AND CONFIDENTIALITY RECORD FOR
THESIS IN THE ACADEMIC REPOSITORY

1.- IDENTIFICATION OF THE ACADEMIC WORK

Type of monograph (check one): ☐ Thesis / Final Project ☒ Thesis (Master/PhD)

Title of the work: Experimental Evaluation and Modeling of Leaching Kinetics and Fine Particle Challenges in Sodium Chloride and Sulfuric Acid Solutions for Lithium-Ion Battery Recycling Plant Design

Candidate's name: RUVI JADE CUBAROL MARAÑAN

Program / Degree: Magíster en Ciencias de la Ingeniería Química

Campus: Casa Central Valparaíso **Department:** Ingeniería Química y Ambiental

2.- VALIDATION BY THE ADVISOR / THESIS DIRECTOR

I, CLAUDIO ABRAHAM ACUÑA PEREZ, in my capacity as Advisor/Director of the academic work mentioned above, hereby **CERTIFY** that:

- I have reviewed this document, and it corresponds to the final approved version of the work.
- The work meets the academic and formatting requirements established by the institution.

3.- CONFIDENTIALITY EVALUATION FOR INDUSTRIAL PROPERTY (check one)

☒ The work DOES NOT contain information that warrants confidentiality and may be published immediately in the open-access repository.

☐ The work CONTAINS information with potential industrial or intellectual property implications and requires a confidentiality period (**embargo**) for (check one):

☐ 6 months ☐ 12 months ☐ 2 years ☐ 3 years ☐ 5 years ☐ 10 years

Justification for the need for confidentiality (mandatory if an embargo is requested):

4.- SIGNATURES

Advisor or Director of the project/thesis:

Date: 24/04/2026 **Signature:** 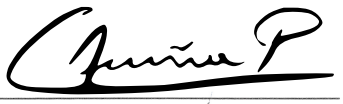

Student or Candidate:

Date: 24 April 2026 **Signature:** 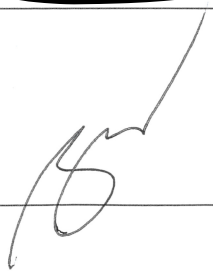

FACULTY OF TECHNOLOGY, OULU MINING SCHOOL, UO

DEPARTMENT OF MINERAL RESOURCES ENGINEERING, MUL

FACULTY OF MINING, GEOLOGY AND PETROLEUM ENGINEERING, UNIZG

DEPARTMENT OF CHEMICAL AND ENVIRONMENTAL ENGINEERING, USM

Experimental Evaluation and Modeling of Leaching Kinetics and Fine Particle Challenges in Sodium Chloride and Sulfuric Acid Solutions for Lithium-Ion Battery Recycling Plant Design

Ruvi Jade Cubarol

DEGREE PROGRAMME EMJM-PROMISE

Erasmus Mundus Joint Master in Sustainable Mineral and Metal Processing Engineering

June 2024

UNIVERSIDAD TÉCNICA FEDERICO SANTA MARÍA

DEPARTMENT OF CHEMICAL AND ENVIRONMENTAL ENGINEERING

VALPARAISO, CHILE

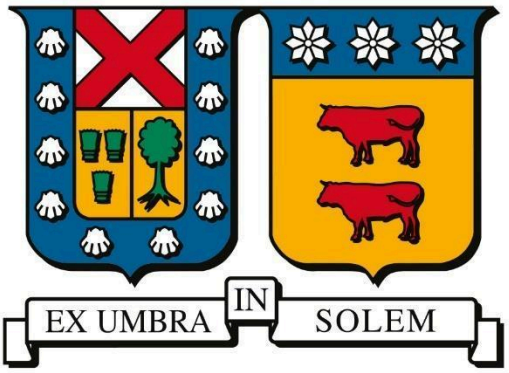

"Experimental Evaluation and Modeling of Leaching Kinetics and Fine Particle Challenges in Sodium Chloride and Sulfuric Acid Solutions for Lithium-Ion Battery Recycling Plant Design"

Ruvi Jade Cubarol

THESIS TO OBTAIN THE DEGREE OF MASTER OF SCIENCE IN CHEMICAL ENGINEERING

Main supervisor: Claudio Acuña Pérez

Co-supervisor: Luis Vinnett Peralta

External supervisor: Julio Valenzuela

Joint Master Erasmus Mundus

June 2024

ABSTRACT

Electromobility's growth for CO_2 reduction has driven the demand for lithium-ion batteries (LIBs), which led to an increasing demand for Li, Co, and Ni with an imminent risk for production shortages. Recycling these spent batteries can mitigate production shortages, as well as disposal issues in landfilling. However, the rheology and composition of LIBs for recycling provided difficulties in the processing. The particle size distribution of LIBs provided high shear stress in the solid-liquid reactors, causing an increased water consumption from the high volume of feed material, including a significant amount of graphite, which also created difficulty in extracting metals. Thus, the study aims to evaluate leaching kinetics for spent battery recycling in different operating parameters for scale-up methodology.

Due to the rheology of fine particles in leaching, a material with similar particle size was used in leaching, which was the smelter flue dust. Different leaching parameters were varied, such as temperature, pulp density, and agitation speed, to determine the optimal parameters for reactor scaling up. High leaching recoveries were achieved with 90°C, 10% solids, and 0.68 m/s tip speed. However, upon scaling up, maintaining the impeller Re minimized the recovery due to an inefficient mixing and suspension of fine particles.

Different kinetic models were assessed based on the σ of experimental and model values and their error distribution from the bench-scale tests of NaCl-H_2SO_4 leaching. The first-order diffusion-controlled model, using R_∞, k, and α, provided a better fit to describe the kinetic data with a mean σ of 0.83±0.1645. The high recoveries of Li, Co, and Ni from the diffusion reaction in the bench-scale tests achieved 970 mV potential of the solution in which a model was created using a neural network with the parameters – temperature and NaCl and H_2SO_4 concentrations. This exhibited that NaCl could increase the oxidizing potential of sulfidic leaching by generating a Cl_2 byproduct for battery recycling achieving high maximum metal recoveries. Utilizing the provided battery recycling simulation from Aspen Plus, it was determined as technically and economically feasible in specific conditions; however, further modifications are required to exhibit actual kinetic data, especially when handling finer sizes.

Keywords: battery recycling, fine particle leaching, sodium chloride, oxidation-reduction potential, kinetic modeling

FOREWORD

The main goal of this study is to provide insights into the leaching kinetics of fine particles and the influence of NaCl addition on the leaching process, particularly in battery recycling applications. This research was conducted over six (6) months as a requirement for obtaining the diploma through the Erasmus Mundus Master Program in Sustainable Mineral and Metal Processing Engineering, a collaborative effort among three partnered universities.

I would like to express my heartfelt gratitude to all those who supported me in completing this research. My sincere thanks go to Prof. Acuña for his unwavering support, guidance, and patience during the development and completion of my study. His warm welcome and assistance in accommodating me in Chile were greatly appreciated. I am also deeply grateful to Ms. Peña, Ms. Gonzalez, Ms. Medina, Mr. Pinto, and the IQA staff for their invaluable assistance with laboratory preparation and activities and for their support as I adjusted to the university environment. Special thanks to Prof. Valenzuela, Mr. Serrano, and UCN for assisting with my requests for information and analysis. Kudos to Francisco, Sebastian, Benjamin, Dylan, and Felipe for their help and assistance.

Additionally, I extend my appreciation to the EMJM PROMISE Consortium for providing me with the opportunity and support to pursue this program and travel the world. To my friends, who were there to cheer in my struggles before, during, and after the study. Finally, I am profoundly thankful to my family, who were a phone call away.

Valparaiso, 27.06.2024

Ruvi Jade Cubarol
Author

TABLE OF CONTENTS

APPENDICES

1 INTRODUCTION

1.1 Background of the study

Global carbon emissions have significantly increased by 50% since 1990, and transportation has contributed 25% of this (International Energy Agency 2024). Combustion engines for vehicles using coal and fuels started in the 1990s, producing carbon dioxide, which causes heat to be trapped inside the atmosphere. This caused car and bus manufacturers to produce electric vehicles (EVs) by powering them with lithium-ion batteries (LIBs) due to their high energy density. However, this transition to electromobility demanded more critical raw materials of lithium, cobalt, and nickel, which compose LIBs, which projected a shortage in raw material production.

The life cycle of LIBs can reach up to 10 years before it is finally disposed of. Initially, the standard use for EVs is above 80% of its performance. Once it fails to reach the requirement, it is then used as an energy storage system requiring less frequent battery cycling of 100-300 cycles per year until it reaches 20% for it to be delivered to a recycling firm before its landfill disposal (Zhao 2017). Considering that batteries consist of heavy metals and electrolytes, toxic material generation from landfills could impose an environmental risk. Thus, diverse recycling technologies have been proposed to minimize the contamination of toxic elements and the shortages in the production and demand of raw materials.

Common LIBs recycling involves dismantling, discharging, shredding, and separating plastics, metal shells, electrolytes, graphite (20%), and fine particle oxides (30%). The fine particle oxides are the cathode active material of a battery composed of lithium metal oxides (LMOs) – $LiCoO_2$ (LCO), $LiMn_2O_4$ (LMO), $LiNiMnCoO_2$ (NMC), $LiNiCoAlO_2$ (NCA), or $LiFePO_4$ (LFP). Once the principal components (graphite and metal oxides) are separated, pyrometallurgical and hydrometallurgical processes are implemented to extract the critical metals further.

Pyrometallurgical processes remove graphite, electrolytes, and plastics at high temperatures and produce metal alloys and slags. This metal alloy contains Co, Ni, and Fe in the process, which is further processed in hydrometallurgy, and the slag recovered comprises Al, Mn, and 82% of Li (Oosterhof and Dupont 2018; Klimko et al. 2020). Slags

are currently used as aggregates with 3-7% Li and require a high mechanical and chemical effort to separate due to their silicate structure (Heimes et al. 2023). It is a simple process operation with no requirement for input size; however, a large volume of waste gas, CO_2, is produced, which would require off-gas treatment and has a high energy consumption.

In contrast, the hydrometallurgical route can recover above 95% of critical elements using strong acids and reducing agents without high consumption of thermal energy and waste gas production. However, the presence of graphite adds volume to the feed, requiring more water and acid consumption, and the removal has yet to be solved on an industrial scale. In addition, its size, including the LMOs, is considered a fine material (< 15 µm), which causes high shear stress in the solid-liquid leaching reactors, reducing reactor capacity.

A review from Jung et al. (2023) on different leaching experiments for batteries showed an increased recovery of the metals with hydrogen peroxide addition in sulfuric acid leaching, promoting the kinetics and dissociation of the metals into the aqueous phase. The use of reductants facilitated the reduction of Co^{3+} (from solid species) to Co^{2+}, which is readily dissolved in aqueous solutions. The effect of increased Co recovery is also observed in Serrano (2022), with the mixture of sulfuric acid and sodium chloride yielding > 92%; however, the effect of NaCl in the leaching conditions was not further discussed.

Chalcopyrite leaching, known to have low Cu extraction rates due to mineral passivation on the particle surface, yielded above 91% with the NaCl addition (Padilla et al. 2003; Carneiro and Leão 2007; Navarro et al. 2020; Quezada et al. 2021). The NaCl affected the porosity and surface area of the material, forming a porous and crystalline sulfur, which improved the extraction kinetics and diffusivity of the acid reagents (Carneiro and Leão 2007).

Thus, it is hypothesized that using NaCl in acid leaching improves the kinetics of leaching and maximizes extraction efficiency, generating an oxidant by-product under battery leaching conditions.

1.2 Objectives of the study

The main objective of this study is to evaluate the kinetics of leaching for spent batteries in varying operating parameters for scale-up methodology. Specifically, it aims to:

1. Assess and analyze the kinetic model of the bench-scale tests from different reagents;
2. Investigate the mechanism of acid and sodium chloride addition in leaching conditions, i.e., oxidation-reduction potential;
3. Evaluate the varying parameters in fine particle leaching based on the extraction efficiency;
4. Evaluate a process design for battery recycling with a technical-economic evaluation.

1.3 Scope and limitations

The study will evaluate leaching kinetics from the bench-scale tests by assessing their reaction rates, mechanism, and extraction efficiencies. It will also delve into the effects of NaCl addition in acid leaching, focusing on the oxidation-reduction potential that influences the process. The impact of varying parameters such as solid concentration, temperature, agitator speed, and volume scale-up will be analyzed using the powder material (flue dust) from a steel scrap recycling plant. Based on these findings, the study will evaluate a process design outlining the optimal operating conditions and parameters from Aspen Plus, evaluating its economic feasibility.

2 LITERATURE REVIEW

The extraction of critical materials from lithium-ion batteries has garnered significant attention due to the increasing demand for sustainable and efficient recycling methods. This literature review focuses on handling fine particles, such as battery materials for leaching extraction, the use of chlorine media in acid leaching, and the different kinetic models that can be applied for leaching kinetics, which are important aspects for maximizing recovery rates.

2.1 LIBs

Lithium-ion batteries have become the most in-demand technology for the green transition due to their large energy density compared to other battery types for electromobility. Lithium, as the main component in the battery, is a light metal with a low electrochemical potential, making it more reactive than the other metals, which is ideal for EVs (Berg 2015).

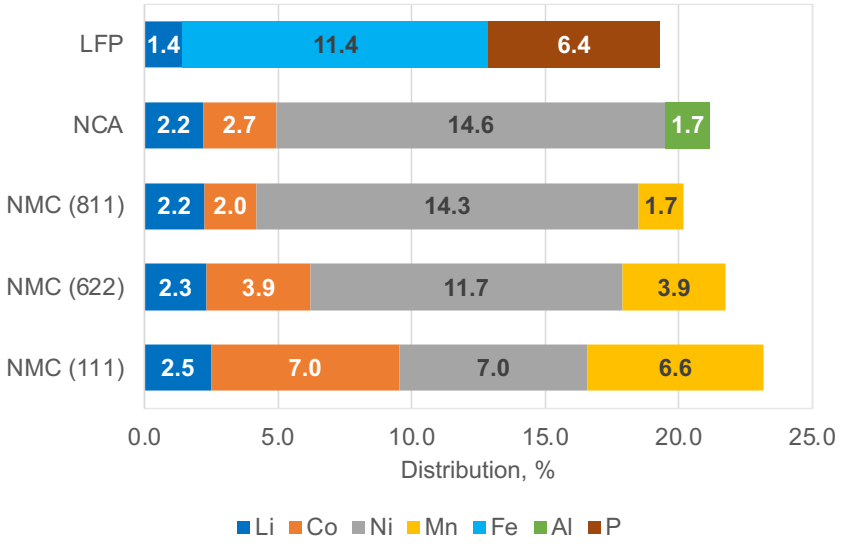

Figure 1. The elemental distribution of Li, Co, Ni, Mn, Fe, Al, and P per battery type (Dai et al. 2019; Ali et al. 2021; Sommerville et al. 2021; Heimes et al. 2023).

More than 50% of the battery composition comprised the anode and the cathode. The anode is the negative electrode, composed of graphite materials where the oxidation reaction occurs, while the cathode is the positive electrode at which the reduction occurs. LIB properties are contributed by the material composition present in their cathode material. The different compositions shown in Figure 1 correspond to their applications

based on thermal stability and energy density. NMC and NCA battery types are commonly used for electric vehicles due to their high energy density and thermal stability, and the LFPs have lower energy density but are the most thermally stable and high-energy cycle for EVs, while LCO and LMO are for electronic devices and power tools (Flash Battery srl 2022).

It is estimated that the global battery demand by 2030 will rise to 2,333 GWh, 10 times the 2020 demand Field (World Economic Forum 2019), creating shortages in global production. The decreasing supply and demand of Li, Co, and Ni in Figure 2 would significantly continue to decrease if the recycling of spent batteries were not accounted for (Lin et al. 2023). Considering that the average service life of EV batteries is 8-10 years, it is expected that 174 GWh will reach its end-of-life and be available for recycling. Due to the large demand in battery (Li, Co, and Ni) and steel (Ni) industries, metal prices have steadily increased. However, current battery prices have become cheaper as battery production technologies have significantly improved by 70% less than the 2015 price (International Energy Agency 2021).

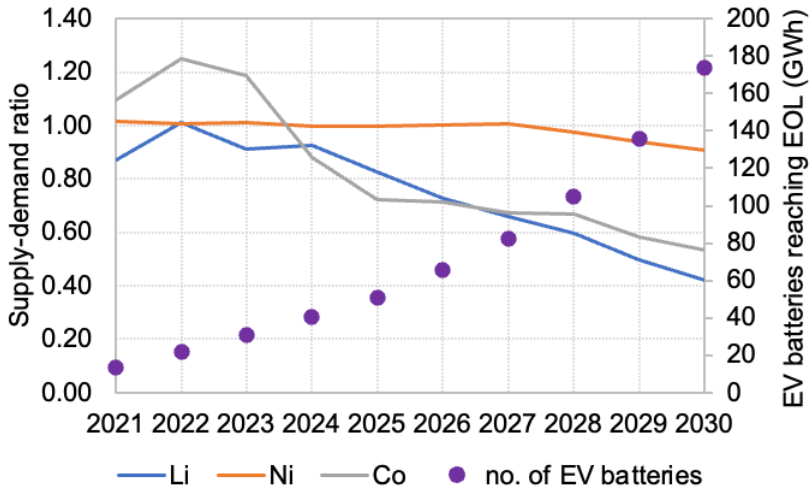

Figure 2. Supply and demand ratio of Li, Co, and Ni and the number of EOL batteries (Lin et al. 2023).

Given the pace of the demand and the market price, recycling batteries could reduce the global demand for 25% of newly mined Li, 25% for Co, and 35% for Ni (Dominish et al. 2021). Thus, different strategies and stages are still being studied to recover these metals efficiently.

2.2 Particle size distribution of LIBs and suspension rheology

LIBs undergo several stages for pre-processing and concentration – dismantling, discharging, size reduction, and classification to produce a final product mainly composed of anodic and cathodic materials. To fully understand the succeeding extraction stages, Shimadzu Corporation (2022) and Xuan et al. (2019) described the particle size distribution of the NMC cathode and graphite materials in Figure 3. The mean particle size of these materials was classified as 15 µm based on their volume distribution which belonged to the size class range of fine sizes defined in the classification of Sivamohan and Forssberg (1985) and Somasundaran (1980). The particle size and the size distribution influence the electrochemical performance of the batteries through the contact and reaction between the anode and cathode materials. This provided a short diffusion pathway for Li ions to travel; thus, the narrower the particle size distribution of the electrodes, the better the cycle stability of a battery (Sheu et al. 1997). However, the particle size of the electrode materials contributed to the rheological characteristics in recycling.

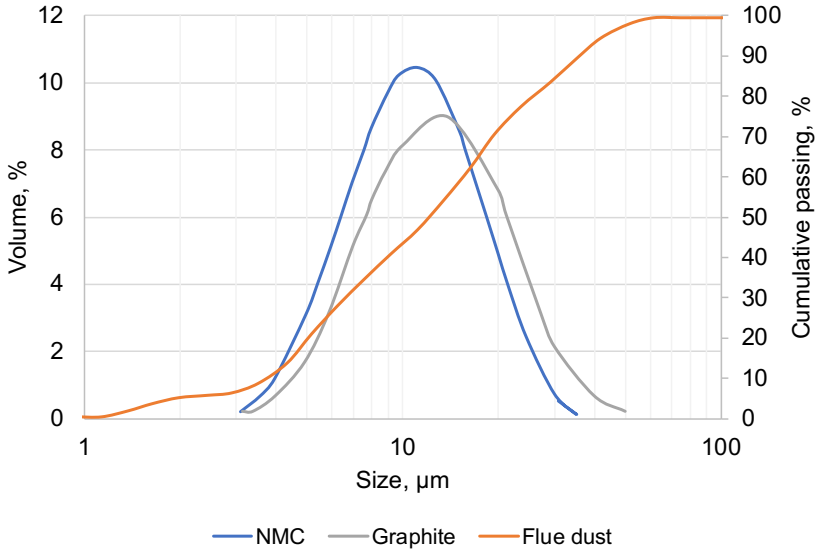

Figure 3. Particle size distribution of NMC cathode and graphite materials in volume distribution against weight distribution of smelter flue dust (Xuan et al. 2019; Chen et al. 2020; Shimadzu Corporation 2022).

A similar size distribution of cathode material was attributed to a smelter flue dust presented in cumulative weight by Chen et al. (2020) in Figure 3, in which the d_{50} was measured to < 15 µm. These dusts were carried away as furnace off-gas and were collected in a dust collection facility. Flue dust generated from an electric furnace was measured by Contreras (2017) with a mean particle size of 10 µm through a sedimentation

test, where the particle size is a function of sedimentation velocity and Reynolds number. The mean particle size of flue dust provided comparable rheological characteristics to battery cathode materials in the pulp behavior for solid-liquid reactors, specifically the solid-to-liquid ratio relevant in metal extraction.

Liu et al. (2021) discussed the effect of the particle size distribution for fine particles on the shear rate and viscosity of the concentrated suspension. As the particle volume fraction increased, it exhibited more shear-thinning characteristics. A comparison between volume fractions of solids relative to their shear rates and stress in a suspension was shown in Figure 4 for silica particles with d_{32} of 14.32 µm. A higher pulp density acted as a non-Newtonian fluid. Thus, the increase in apparent viscosity of the pulp would require more shear stress to maintain the suspension of finer particles. The shear stress was generated by the agitators/mixers.

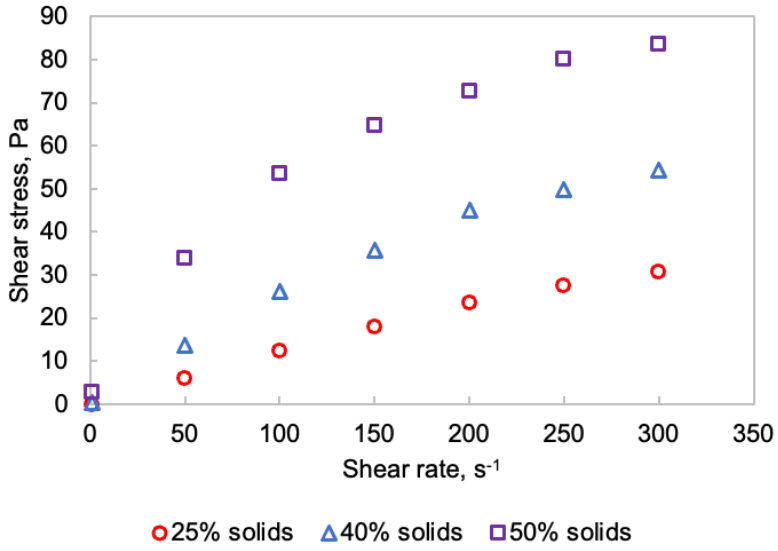

Figure 4. The relationship between shear stress and shear rate of fine particle suspensions at different volume fractions (Liu et al. 2021).

Mixing fluids accelerated the blending and uniformity of materials for diffusion and chemical processes. However, scaling up fluid mixing for fine particles in the solid-liquid reactors has been a problem because the shear rate of the fluid varies the apparent viscosity. Typical non-Newtonian fluids were in laminar mixing conditions as the process parameters have an effect on fluid behavior described by the Reynolds number, Re (Green and Perry 2008; Triveni et al. 2010). In scaling up, if Re was maintained to keep the similarity of both scale and upscale, the impeller speed would be reduced and more likely increase the apparent viscosity, which was not ideal for fine particle suspension. The common criterion for scaling up industrial mixers is the tip speed, which was calculated

as πDN, where D the impeller diameter and N the rotational speed. Maintaining a constant tip speed was identical to constant torque per unit volume which keeps the liquid in motion at a reasonable amount of power consumption (Triveni et al. 2010).

To address issues in handling fine particles, it also important to identify the components present in the material. By understanding the size distribution and physical characteristics, processes can be tailored to minimize shear distribution inside reactors. This approach also facilitates the potential reuse of the material without altering its properties.

2.3 Graphite removal

Graphite comprises 20% of LIBs as an anode, providing high conductivity, performance, and charge capacity. Due to its high importance in other applications, such as solar panels and aerospace, it has gained more importance in recycling spent LIBs. This can be recovered through leaching in battery recycling as residue, but due to its particle size distribution, as described previously, it has provided more challenges in the recovery of critical metals in leaching as it created more viscosity in the solid-liquid suspension (Porvali et al. 2019) and contributed to the increased feed material volume requiring more reagent consumption and water in the process (Vanderbruggen et al. 2022). However, technologies have emerged to remove graphite before the metal extraction process – flotation.

The separation of graphite can be feasible through flotation due to its natural hydrophobicity. However, the use of direct flotation on fine particles achieved low recoveries. A study by Kohmuench et al. (2018) showed a trade-off in the recovery of metal sulfide from different industrial flotation plants at particles < 20 μm. These particle sizes were inefficiently recovered by flotation because of the reduced probability of mineral and bubble collision and the effect of the mineral's small mass easily repelled by the forces of agitation.

Arriagada et al. (2020) provided a new technology to improve the recovery of fine particles in flotation, which used hydrophobized glass bubbles as carriers produced through the esterification of commercial glass bubbles. A 30% increase in the recovery was observed in Figure 5 in the addition of hydrophobized glass bubbles. The use of these

glass bubbles in the flotation of fine particles promoted the selective particle agglomeration of the fine graphite, requiring no addition of frothers. However, from the study of Vanderbruggen (2022) on the flotation behavior of LMOs and graphite for recycling, the hydrophobicity of graphite was comparatively higher than that of the LMOs characterized by their wettability. This implied that LMOs could not be identified as hydrophilic even if the organic binder was fully liberated from the black mass. Without the use of a depressant or selective collector, there is a significant probability of the LMOs reporting in the froth phase along with the graphite.

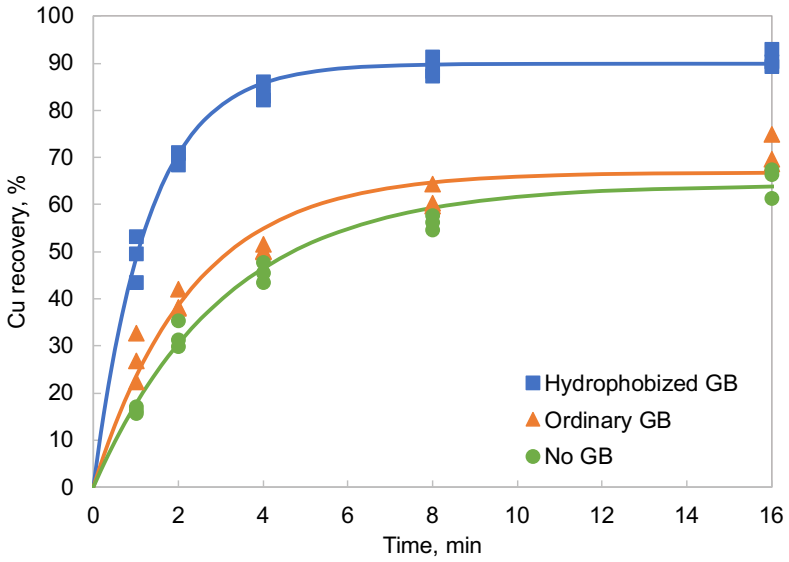

Figure 5. Cu recovery in a glass bubble flotation fitted in a first-order kinetic model (Arriagada et al. 2020).

This new technology enhances flotation efficiency while simultaneously reducing reagent consumption during the leaching stage due to decreased feed volume. Using glass bubbles in the flotation of fine particles presents a new insight for the efficient recovery of graphite from spent LIBs. However, further investigation into the impact of organic binder on the flotation is necessary to optimize its recovery.

2.4 Acid leaching of LMOs

Leaching was used to extract metals from spent batteries after the mechanical and physical separation. A summary review by Jung et al. (2022) used different types of acids in extracting LMOs – hydrochloric acid, nitric acid, and sulfuric acid, the most used as leaching reagents. However, using these inorganic acids could generate toxic gases such

as Cl_2, SO_3, and NO_x at specific leaching conditions. Respective reactions of acids to LMOs were illustrated in Equations 1 to 4.

$$2LiCoO_2 + 8HCl \rightarrow 2LiCl_{(aq)} + 2CoCl_{2(aq)} + 4H_2O + Cl_{2(g)} \quad (1)$$

$$4LiCoO_2 + 12HNO_3 \rightarrow 4Co(NO_3)_{2(aq)} + 4LiNO_{3(aq)} + 6H_2O + O_{2(g)} \quad (2)$$

$$6LiCoO_2 + 6H_2SO_4 \rightarrow Co_3O_4 + 3Li_2SO_{4(aq)} + 3CoSO_{4(aq)} + 6H_2O + O_{2(g)} \quad (3)$$

$$4LiCoO_2 + 6H_2SO_4 \rightarrow 4CoSO_{4(aq)} + 2Li_2SO_{4(aq)} + 6H_2O + O_{2(g)} \quad (4)$$

An acid leaching of computer batteries from Serrano (2022) using 2M H_2SO_4 yielded recoveries of Li, Ni, and Co at 57%, 62%, and 38%, respectively. This low recovery, especially of Co from the LMOs, was attributed to the formation of Co_3O_4, which was not dissociated into soluble ions of Co^{2+}. The acidity and oxidation-reduction potential (ORP) of the process are essential in the leaching process to achieve an efficient recovery. The ORP was characterized by an exchange of electrons from the dissociation of solid metals, producing electrons to form metal ions (Dusing et al. 1992).

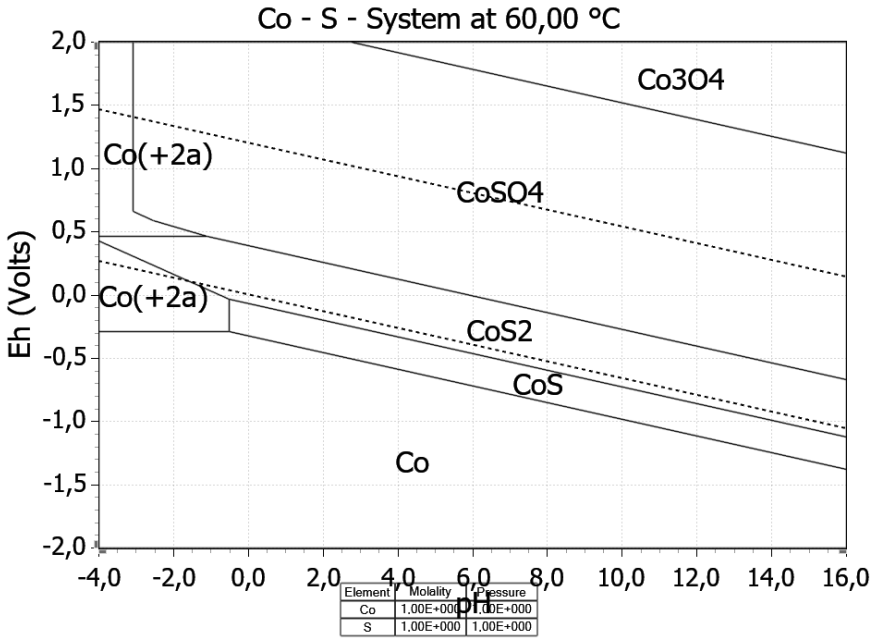

Figure 6. Eh-pH diagram of Co in H_2SO_4 system at 60°C using HSC Chemistry® 10.

As described in Equation 3, Co_3O_4 was formed first in the H_2SO_4 leaching, which would require an excess of H_2SO_4 to convert to soluble $CoSO_4$ (Ferreira et al. 2009). In the Co-H_2SO_4 system prepared in HSC Chemistry® 10, Figure 6, Co^{2+} tends to form at lower pH

values at a specific oxidizing-reducing condition. which would require more H^+ ions from the acid, increasing the reagent consumption. The increasing amount of H_2SO_4 added to the solution to lower the pH values can also increase the oxidation potential of the solution (Racyte et al. 2009). However, the high acid consumption at an industrial scale could increase the overall reagent consumption, which is not economical.

2.5 Oxidation-reduction potential in leaching

A study from Aaltonen et al. (2017) described the reducing conditions in Figure 7 based on the ORP, measured in mV, at different concentrations of H_2O_2. The reducing conditions of H_2O_2 facilitated the reduction of Co^{3+} to Co^{2+}, as shown in Equation 5 (Jung et al. 2022). Chen and Ho (2018) supported the effect of ORP in the recovery of Li, Co, and Ni, where the increasing concentration of H_2O_2 provided increasing recoveries.

$$Co_3O_4 + 3H_2SO_4 + H_2O_2 \rightarrow 3CoSO_{4(aq)} + 4H_2O + O_{2(g)} \quad (5)$$

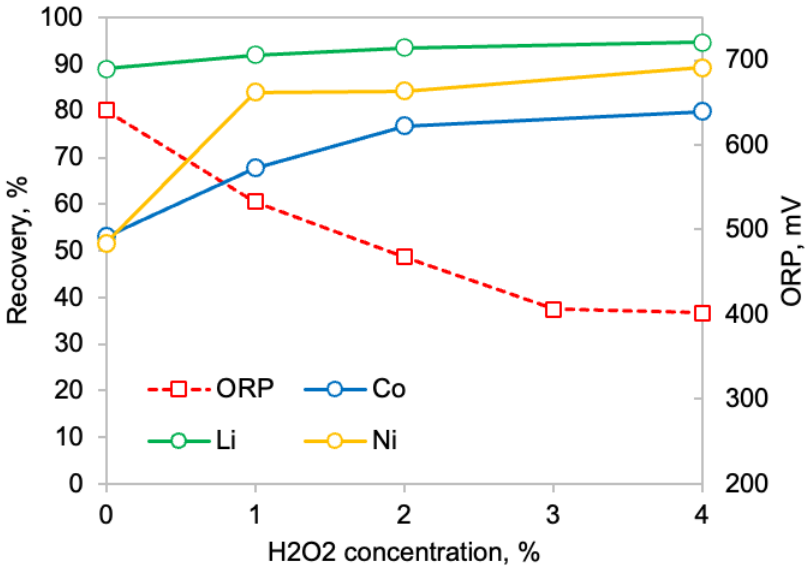

Figure 7. Yield recovery of Li, Ni, and Co at varying H_2O_2 concentrations (Aaltonen et al. 2017; Chen and Ho 2018).

Other compounds were studied using glucose and ascorbic acid as reducing agents, which decreased the ORP to 600 and 300 mV, respectively (Aaltonen et al. 2017). The effect of the addition of ascorbic acid in H_2SO_4 leaching provided selective leaching on Li and Co, where it inhibited the recovery of Cu along with the increased concentration of the additive (Peng et al. 2018). The decrease in Cu recovery and increase in Li and Co

recovery were reflected in the reduction of ORP from 770 to 60 mV. The reducing conditions of the acidic media influenced the leaching mechanism.

In the field of electrolytic processes, two products – electrolyzed reducing water and electrolyzed oxidizing water, were produced by electrolyzing water with chlorine salt, typically with sodium chloride. Due to the economic feasibility and availability of NaCl, it has been the most used chlorine salt for electrolyzing. In the process, the positively charged ions, Na^+ and H^+, move to the cathode, generating NaOH and H_2 gas to produce reducing water, while the negatively charged ions transfer to the anode, forming HClO, ClO^-, HCl, O_2, and Cl_2 for oxidizing water (Prasakti et al. 2022). It has been known that O_2 and Cl_2 are oxidizing agents with an oxidation potential of 1.23 and 1.36 V, respectively (Lincho et al. 2021). High ORP values were produced in the anode products, which provided oxidizing conditions, as shown in Figure 8. The increasing NaCl concentration in the solution also increases the potential at longer periods due to the large volume of oxidants produced in the process.

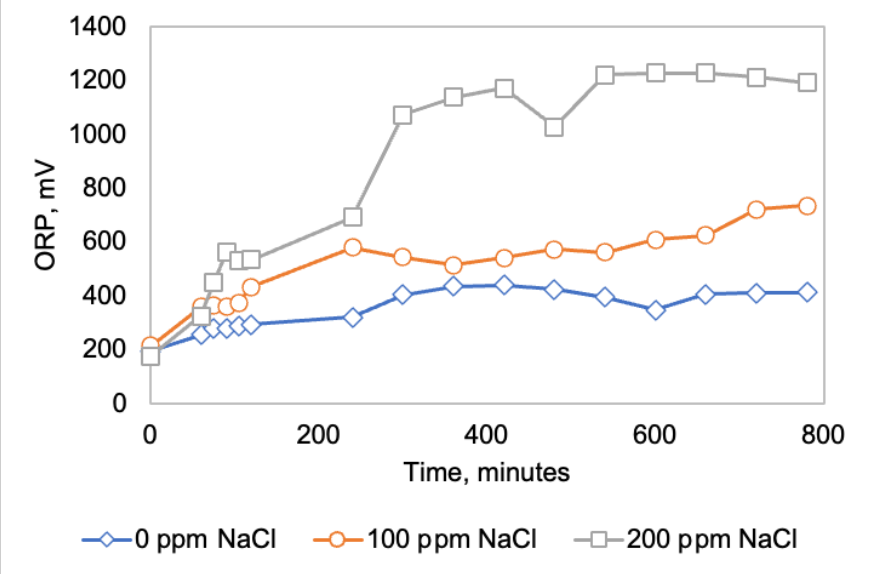

Figure 8. ORP values of the electrolyzed oxidizing water at different NaCl concentrations (Prasakti et al. 2022).

The increase in ORP from the electrolytic process of salt solution exhibited an approach to promote the production of oxidants. These characteristics showed potential applications of chloride media in leaching processes to enhance metal dissolution at oxidizing conditions. Leveraging its efficient capabilities, it presented a possible approach to improve metal extraction processes based on its potential.

2.6 Addition of NaCl in leaching

Chloride ions were used in the Cuprochlor® process, where copper sulfides were leached using calcium chloride in the agglomeration stage for heap leaching. Adding $CaCl_2$ improved the oxidizing conditions in obtaining rapid solubilization of copper sulfides during the curing and, therefore, improved the extraction of copper in the leaching (Neira et al. 2021). Under the working conditions of Mineral Michilla in Chile from the patent of Alfaro et al. (2005), the total copper extraction rate was 90% in a leaching time of 110 days.

In the study of Hernández et al. (2019), using sodium nitrate and sodium chloride in the pre-treatment stage provided oxidizing conditions in the 30 days of curing. A copper extraction rate of 63% was achieved by adding sodium nitrate and chloride during the column leaching. The reactions in Equations 6 and 7 showed the response of copper sulfides towards the addition of reagents in H_2SO_4 leaching.

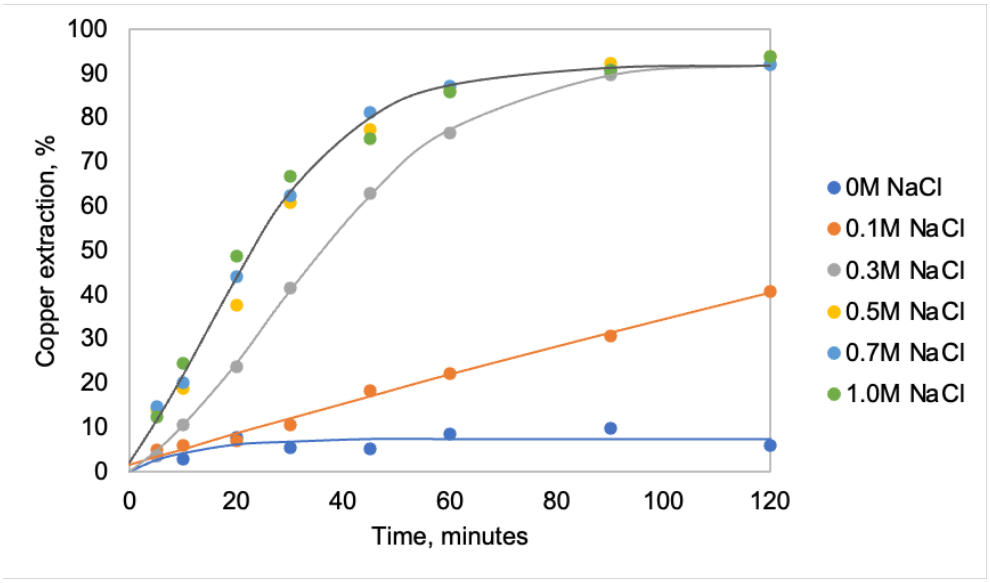

Figure 9. The effect of varying NaCl concentrations on the copper extraction at 0.6M H_2SO_4, 0.3% solids, and -53 +45 µm (Padilla et al. 2003).

$$2CuFeS_2 + 10H_2SO_4 + 10NaNO_3 + 4NaCl \rightarrow 2CuCl_2 + Fe_2(SO_4)_3 + 10NO_2 + 4S + 10H_2O + 7Na_2SO_4 \quad (6)$$

$$3CuS + 4H_2SO_4 + 2NaNO_3 + 6NaCl \rightarrow 3CuCl_2 + 2NO + 3S + 4H_2O + 4Na_2SO_4 \quad (7)$$

In addition, Padilla et al. (2003) discussed that the chloride ion concentration in Figure 9 increased the copper extraction in chalcopyrite leaching. The kinetics of leaching in concentrations greater than 0.5 M achieved high recoveries but did not show a significant increase in the extraction. It was determined that the copper dissolution during leaching does not form a sulfur layer on the particle surface. Carneiro and Leão (2007) further concluded that the chloride ions affect the chalcopyrite leaching with ferric sulfate by changing the sulfur layer morphology into porous and crystalline, improving the solution's diffusivity. It could be inferred that the waste brine from reverse osmosis could provide a chloride medium for leaching. However, chloride ions could present corrosion problems in the piping and the equipment used in the extraction process from the solutions upon scaling up (Muñoz-Ribadeneira and Gomberg 1971; Ruan et al. 2021).

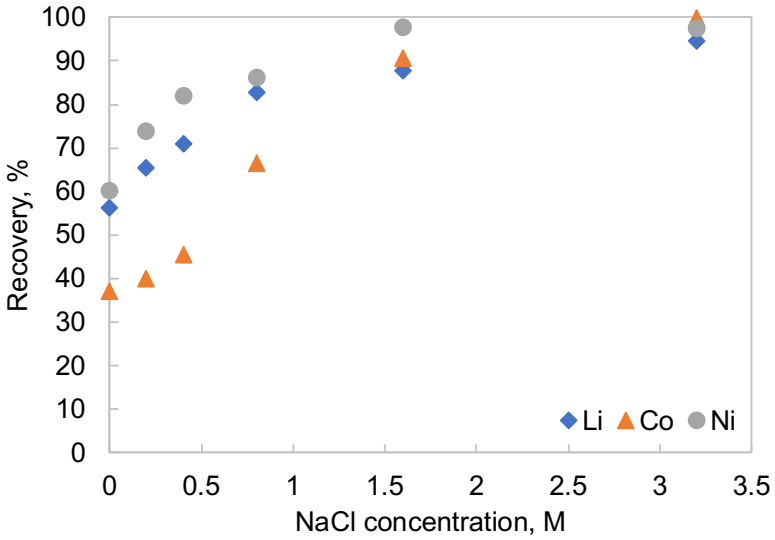

Figure 10. Yield recovery of Li, Ni, and Co with varying NaCl concentration addition in 2M H_2SO_4 leaching at 120 minutes (Serrano 2022).

In a recent study on the leaching of computer batteries by Serrano (2022), NaCl was added to the H_2SO_4 solution. Increasing the concentration of NaCl in Figure 10 in the extraction increased the dissociation of Li, Ni, and especially Co. It was suggested that the dissociation of Co^{3+} to Co^{2+} was caused by the (i) dissociation constant of HCl, which was produced after the addition of NaCl, (ii) the presence of halides (Cl), and (iii) the generation of chlorine gas (Cl_2). However, the oxidizing-reducing conditions of different NaCl additions were not discussed or mentioned in the leaching processes. This will be further elaborated using a model in this research.

To describe the kinetics of leaching tests of NaCl addition, a fitted shrinking core model was used in which the dissociation of the metal ions controlled by diffusion. Since LMOs

have a fine size distribution, the diffusivity of the reagents into the solid surface of the material in the battery leaching was improved due to the increased solid-liquid interfacial area. The ability of the chemicals to diffuse to the material surface supported the leaching kinetics according to the particle size of the material.

2.7 Kinetic models for leaching

It has been commonly used to describe the kinetics of leaching by shrinking core model, in which the grade and degree of mineral liberation were the factors in the extraction. However, the shrinking core model is not applicable in all leaching kinetics as it does not describe the effect of reagent concentration in the dissolution kinetics.

Widely used phenomena to describe flotation chemical kinetics in a batch reactor were modeled in a first-order differential equation to homogeneous chemical kinetics in Equation 8 with C as the concentration of the metal, n the kinetic order, and k as the kinetic rate constant. The classic first-order model was derived from Equation 8 with $n = 1$, which then translates to Equation 9 for the recovery as a function of time where R_∞ was the maximum recovery at time t_∞ and k constant in first-order. Another model used to describe first-order kinetics was a rectangular model or Klimpel model in Equation 10. However, these first-order models presented do not account for conditions such as particle size and differences in physical properties but provided acceptable performance while keeping a low number of parameters (Vinnett et al. 2015).

$$\frac{dC}{dt} = -k \cdot C^n \tag{8}$$

$$R(t) = R_\infty(1 - e^{-kt}) \tag{9}$$

$$R(t) = R_\infty\left[1 - \frac{(1-e^{-kt})}{kt}\right] \tag{10}$$

The use of fractional calculus in modeling kinetics provided support by Simpson et al. (2013) minimizing the number of parameters in fitting models contrary to Fick's model approach. Vinnett et al. (2015) proposed a new method to describe kinetic data based on fractional calculus. The alternative kinetic expression for recovery was described in Equation 11 using three parameters – maximum recovery R_∞ at time t_∞, fractional kinetic order α, and a fractional rate constant k_α, where E_α is the Mittag-Leffler function in

Equation 12. When $\alpha = 1$, Equation 12 translates to $E_\alpha(\mathrm{Z}) = e^{\mathrm{Z}}$ restoring the classic first-order kinetics.

$$R(t) = R_\infty \cdot [1 - E_\alpha(-k_\alpha \cdot t^\alpha)] \quad (11)$$

$$E_\alpha(\mathrm{Z}) = \sum_{i=0}^{\infty} \frac{\mathrm{Z}^i}{\Gamma(\alpha \cdot i + 1)} \quad (12)$$

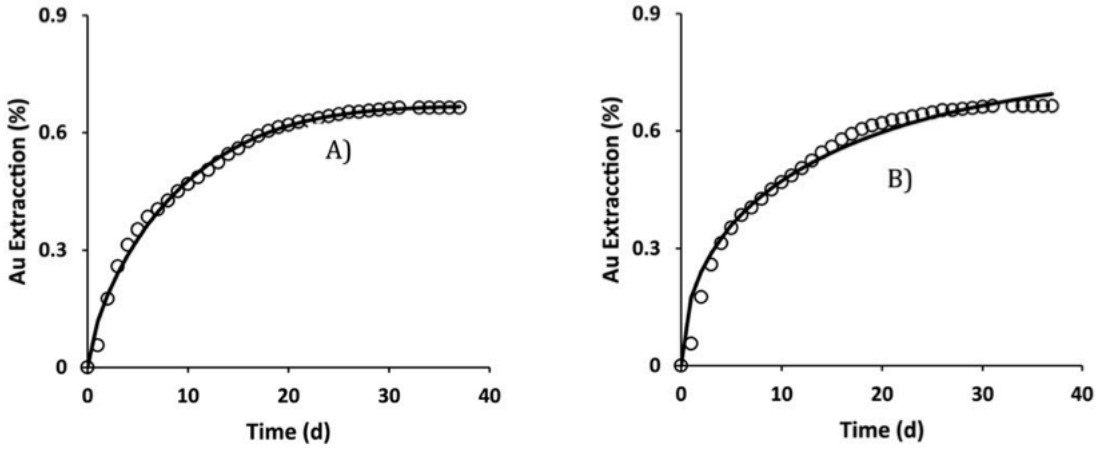

Figure 11. Predicted models (a) fractional model and (b) Fick's model.

A column leaching test from Jacques et al. (2017) provided a higher regression of 0.994 using the fractional model than the traditional model of Fick's model, which was 0.975, as shown in Figure 11. The fractional model demonstrated improved kinetic data estimations without overestimating maximum recoveries. The risk for over-parameterization was minimized when comparing the models by assessing the "goodness of fit" of models both in the statistical quality parameters regression and the adjusted regression. In this case, a fast kinetic dissociation was observed in the first 20 days, followed by a slow dissociation. This effect in the recovery was caused by time-dependent diffusion.

In the current study, the three models will be compared – the first-order model, the Klimpel model, and the first-order diffusion-controlled model modifying Equation 11 with t^α. The selection for the best kinetic model will be based on the residual analysis of the fitting models and their distribution around the mean value.

3 RESEARCH PROCESS

The experimental evaluation included bench-scale leaching tests using sodium chloride and sulfuric acid to assess the kinetic model and understand the leaching mechanisms. To simulate the challenges posed by fine particles in the spent battery material, smelter flue dust with a similar particle size distribution was used, providing a more realistic assessment of the leaching process. The effects of various parameters – temperature, pulp density, and agitation speed on the leaching efficiency and metal extraction (zinc) were investigated.

3.1 Materials preparation

3.1.1 Materials and chemicals

The following materials in Table 1 were used to measure the different processes indicated by leaching tests and mixing of solutions for ORP measurements.

Table 1. Materials and chemicals used in the tests with description.

Material	Description
Flue dust	The dust was obtained from an electric arc furnace in a steel recycling plant in Santiago, Chile.
Sodium chloride	A commercial salt with a sodium amount of 39 g/100 g was used with the brand name LOBOS.
Sulfuric acid	In leaching and ORP measurements, analytical grade sulfuric acid with a purity of 98% and specific gravity of 1.84 g/mL was used.
Hydrochloric acid	An analytical grade hydrochloric acid with 35% purity and a specific gravity of 1.18 g/mL was used in the leaching tests.
Nitric acid	An analytical grade was used with 69-70% purity and a specific gravity of 1.42 g/mL

3.1.2 Equipment description

The following equipment were the potentiometers used to measure the different chemical properties of the tests conducted. These measurements will be used to create a model from varying solutions and validate data.

ORP meter: The oxidation-reduction potential was measured using the San-Xin SX751 meter shown in Figure 12. This type of equipment is a multi-parameter meter that can measure pH, ORP, conductivity, and dissolved oxygen; however, only one electrode can be used at a time. It has a built-in microprocessor chip with automatic temperature compensation and a reference electrode of Ag/AgCl.

Figure 12. San-Xin SX571 meter with ORP electrode.

Figure 13. HI5522 multi-parameter with conductivity, temperature, and pH probes.

pH/Conductivity/temperature meter: The pH, conductivity, and temperature were measured using the Hanna Instruments HI5522 with HI1131 pH probe, HI76312 conductivity probe with a cell constant of 1/cm, and HI7662-W temperature sensor as

shown in Figure 13. This equipment can measure pH, ORP, ion selective electrode, conductivity, resistivity, total dispersed solids, salinity, and temperature. However, the two input channels of the equipment featured one potentiometric sensor and another for electrolytic conductivity. The pH values and conductivity were automatically temperature-compensated upon data collection.

3.2 Research methods

To satisfy the identified objectives, two separate tests were conducted to study the kinetics of leaching – (1) vary different parameters for leaching such as temperature, tip speed, solid-to-liquid ratio in % solids, and increase in volume, and (2) vary concentrations of NaCl addition to H_2SO_4 leaching.

3.2.1 Sample preparation

The 10 kg powder sample obtained was homogenized and divided by coning and quartering method to obtain the representative material of 2.5 kg. A 50 g representative was characterized for the particle size distribution using a laser diffraction particle size analyzer from the university's Chemical and Environmental Engineering Department. Another 50 g was taken for elemental characterization and sent to Universidad Catolica del Norte in Antofagasta using XRF and XRD analyses. It was determined that the density of the material for leaching was 3650 kg/m^3 using a pycnometer.

3.2.2 Leaching test with varying parameters

In a 250-mL beaker, a diluted acid solution was added and then heated to the desired temperature. Agitation was set to the desired tip speed, and the powder material was added to the solution. The setup for leaching was illustrated in Figure 14 using a pitch blade agitator with 4 impellers and a diameter of 5 cm. The leaching was done in 2 hours. Samples were taken at 0, 1, 3, 5, 8, and 120 minutes and were then filtered using Whatman No. 3. When taking the samples, agitation was stopped 30 seconds before the time to allow the settling of the particles and limit the number of solids suspended in the solution to be taken.

One parameter was varied, and the remaining parameters were maintained to observe the varying effects of leaching parameters. See Table 2 for the parameters used in the leaching

tests. The baseline parameter was 2 M H_2SO_4, 60°C, 250 mL, 260 rpm, and 5% solids. However, the solid density was set at 15% for varying the tip speed, and the remaining parameters were maintained according to the baseline. The filtered solution was then analyzed using atomic absorption spectroscopy for zinc.

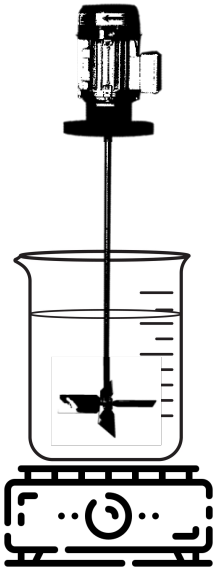

Figure 14. Experimental set-up with the hotplate, beaker, and mechanical agitator.

Table 2. Experimental design for leaching optimization.

Acid type	H_2SO_4	HCl	HNO3
Acid conc, M	2	2	2
Temperature, °C	25	60	80
Volume, mL	250	1000	
Tip speed, m/s	0.42	0.68	0.94
% solids	5	10	20

3.2.3 ORP measurements

In a 1-L beaker, 200 mL of distilled water was added, and pH, ORP, and temperature were measured, as shown in Figure 15 for the set-up. A volume of 237.5 gpl NaCl solution was added to the distilled water, and the pH, ORP, and temperature were measured for 20 minutes. An additional volume of NaCl solution was added in 20, 40, 60, 80, and 100 minutes. The increasing volume addition of NaCl solution indicated an increasing NaCl concentration. The same procedure was followed using 1 M and 2 M H_2SO_4 solutions. Concentrated H_2SO_4 (98% purity) was added in every NaCl addition to maintain the acid

concentration in the solution. The volumes of the added NaCl solution and concentrated H_2SO_4 into the solution were shown in Table 3.

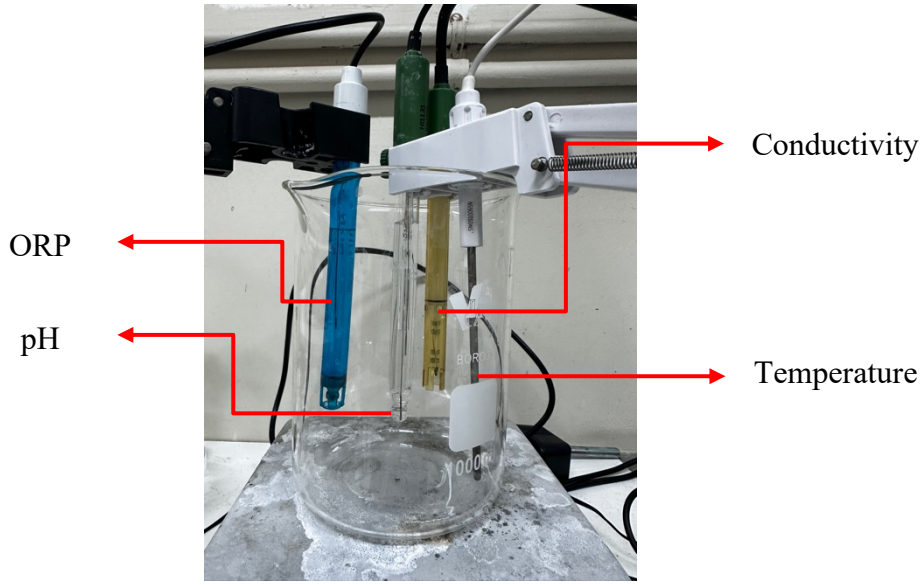

Figure 15. Experimental set-up in measuring the ORP with the continuous addition of reagents.

Table 3. Volume of NaCl solution and H_2SO_4 added in each time interval (in mL).

Time (minutes)	Distilled water	1 M H_2SO_4		2 M H_2SO_4	
	NaCl (mL)	NaCl (mL)	H_2SO_4 (mL)	NaCl (mL)	H_2SO_4 (mL)
0	0	0	11.50	0	24.44
20	8.70	9.22	0.53	9.81	1.20
40	9.49	10.11	0.58	10.82	1.32
60	21.82	23.46	1.35	25.38	3.10
80	60.00	66.09	3.80	73.51	8.98
100	300.00	369.11	21.23	474.51	57.98

3.3 Research analysis

The initial results from the conducted tests and analyses performed by third-party centers provided insights into the efficiency of the leaching process and fine particle handling. These findings serve as a benchmark for evaluating current methodologies and identifying areas for improvement in both laboratory and industrial scales.

3.3.1 Material characterization

Fine materials were leached using the flue dust from a steel recycling plant. The particle size distribution of the material using the Bettersize BT-9300H system with a refractive index of 1.596 ± 0.100i for the powder material was shown in Figure 16. The powder material was composed of < 1 µm based on its frequency distribution calculated from the given volume distribution. By calculating the weight distribution using the density of the material of 3650 kg/m^3, P80 was measured at 28.18 µm. However, the P80 of the material does not consider the sensitivity of the distribution and flow behavior in finer sizes. Since the P80 provided inadequate measurements of the fine size distribution, the mean diameter over volume could be calculated as d_{43}. d_{43} was calculated by Equation 9, where ϕ is the diameter and f is the number of particles of size class i. Therefore, the d_{43} was measured at 13.94 µm.

$$d_{43} = \frac{\sum \phi_i^4 \cdot f_i}{\sum \phi_i^3 \cdot f_i} \tag{9}$$

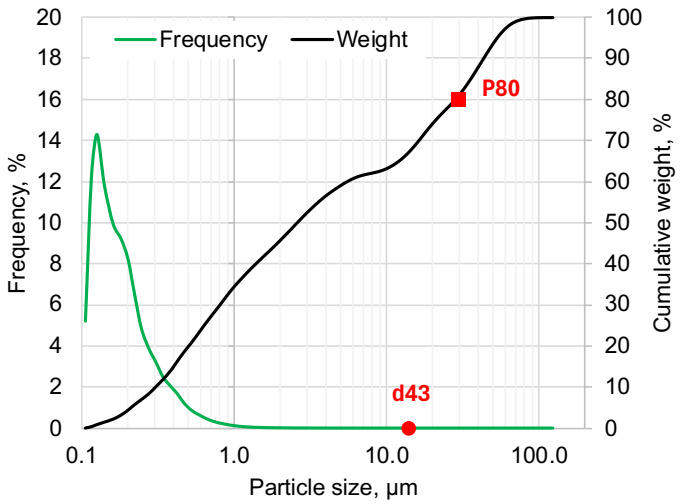

Figure 16. Particle distribution of the fine material according to weight and frequency with P80 and d_{43}.

Elemental characterization of the fine powder material was done using Siemens sequential X-ray spectrometer SRS3000 which showed the distribution in Table 4. This data was confirmed using mineral analysis by Siemens X-ray diffractometer D5000 shown in Table 5. The full list of the elemental and mineral characterization was included in Appendix 2. The main mineral component of the material was an oxide, which indicated no presence of sulfur and carbon. Therefore, calcination was not included in the

pretreatment for the leaching tests. And the feed assay of Zn was used to determine the extraction rates in the conducted fine particle leaching tests.

Table 4. Elemental distribution from XRF analysis.

Zn, %	Fe, %	Pb, %
40.9	21.1	2.34

Table 5. Mineral distribution from XRD analysis with 2θ of 1.5406 in weight distribution, %.

Zincite, ZnO	61.5
Franklinite, $ZnFe_2O_4$	13.6

3.3.2 ORP measurements

Different ORP values were taken to evaluate the conditions of battery leaching tests, showing average measurements every 20 minutes in Figure 17. Low ORP values were attributed to the absence of the acid when increasing NaCl concentration, whereas the acid addition contributed to an increase in ORP by 200 mV, especially at higher concentrations of salt solution. A 143 gpl of NaCl solution and 2M H_2SO_4 measured ORP to 900 mV with a slight pungent smell. Since ORP measurements were not taken from the study of Serrano (2022), a model was provided from the conducted tests to determine the oxidizing-reducing conditions of the bench-scale computer battery leaching tests.

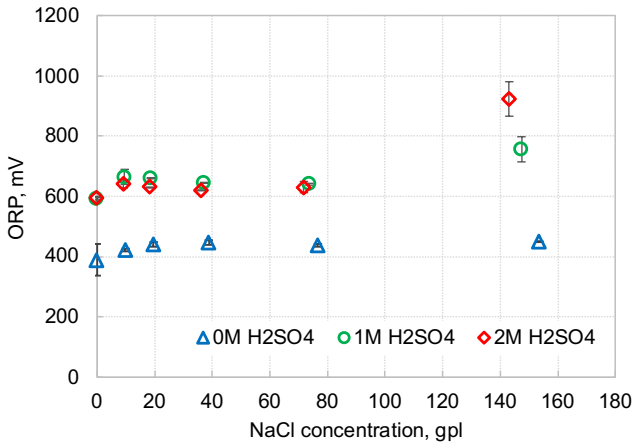

Figure 17. Average ORP measurements at different acid concentrations and increasing NaCl addition.

4 ASSESSMENT OF THE RESULTS

This section presents the experimental evaluation and modeling of leaching kinetics and fine particle challenges in sodium chloride and sulfuric acid solutions for lithium-ion battery recycling plant design. The study assesses the kinetic model of bench-scale tests using different reagents and investigates the mechanism of acid and sodium chloride addition in leaching conditions. The impact of varying parameters such as temperature, pulp density, and agitation speed on leaching efficiency and extraction of target metals (lithium, cobalt, nickel) is also investigated. The results show that high metal recoveries were achieved at optimal conditions, and the first-order diffusion-controlled model provided the best fit to describe the leaching kinetics. The section also discusses the use of a neural network model to predict the oxidation-reduction potential of the leaching solution and the technical and economic feasibility of the proposed battery recycling process.

4.1 Kinetic models from batch-scale tests

Different kinetic models were used to determine the kinetics of computer battery leaching from the bench-scale tests of Serrano (2022) with the addition of varying NaCl concentrations to H_2SO_4 leaching. The models used to compare were taken from Equations 9, 10, and 11, determining the kinetic data referred to in the following discussions as first-order, Klimpel, and first-order diffusion-controlled models, respectively. The diffusion-controlled model was translated to Equation 13, with R_∞ the maximum recovery, k the diffusion constant, and α the fractional order at time t.

$$R(t) = R_\infty \cdot \left(1 - e^{-k \cdot t^\alpha}\right) \tag{13}$$

The kinetic models were obtained by calculating the kinetic parameters restricting R_∞ to not exceed 100. Using the kinetic values, confidence intervals in the time-recovery curve were estimated at the 95% level of confidence using a two-tailed t-test. Recovery values outside the confidence interval were rejected, and the new kinetic data was recalculated to minimize the lack of fit of the model and plot the corrected model within the confidence level. Figure 18 showed the different kinetic models at 2M H_2SO_4 leaching with different NaCl concentrations. Two different colored curves were shown in the plots. The red curve represented the original points in the model with red cross recovery values, while the blue

curve represented the adjusted model with which the recoveries outside the confidence interval were rejected and were replotted with blue round values.

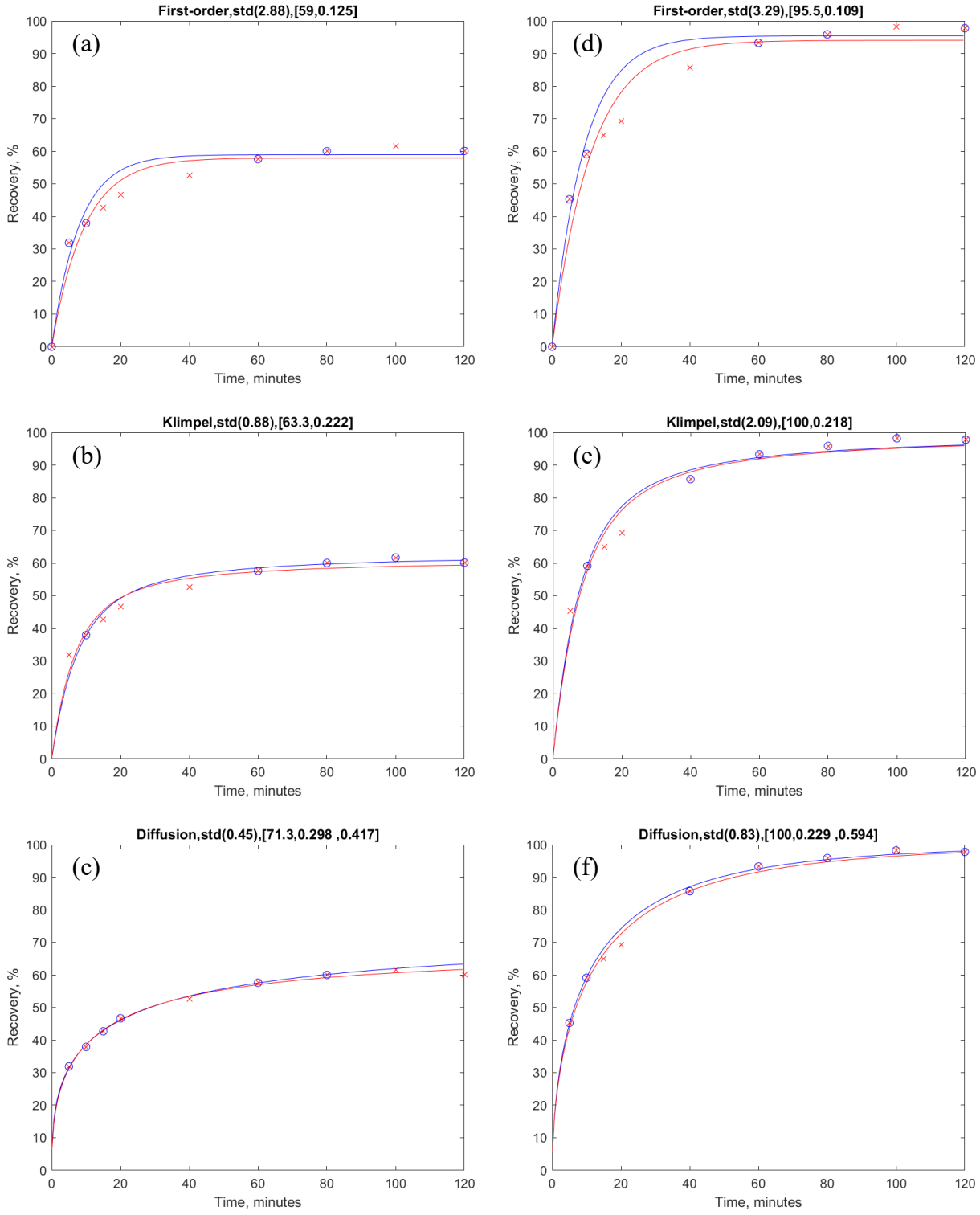

Figure 18. Ni recovery plots of different kinetics models at 2M H_2SO_4 leaching - (a), (b), and (c) 0M NaCl; (d), (e), and (f) 3.2M NaCl. Title notations - kinetic model, σ, [R_∞, k, α].

Determining the modal value of the number of observations used in the adjusted models within the confidence interval, the first-order diffusion-controlled model used 7 values from the 9 observations compared to the other two models of 6 values. This indicated that fewer recovery points were rejected in the first-order diffusion-controlled model than in the first-order and Klimpel models. Comparing the kinetic curves demonstrated in Figure 19 for the Ni recovery in 2M H2SO4-1.6M NaCl, the first-order diffusion-controlled model showed lesser tails between the model and experimental data. However, it was not enough to describe the precision of the model.

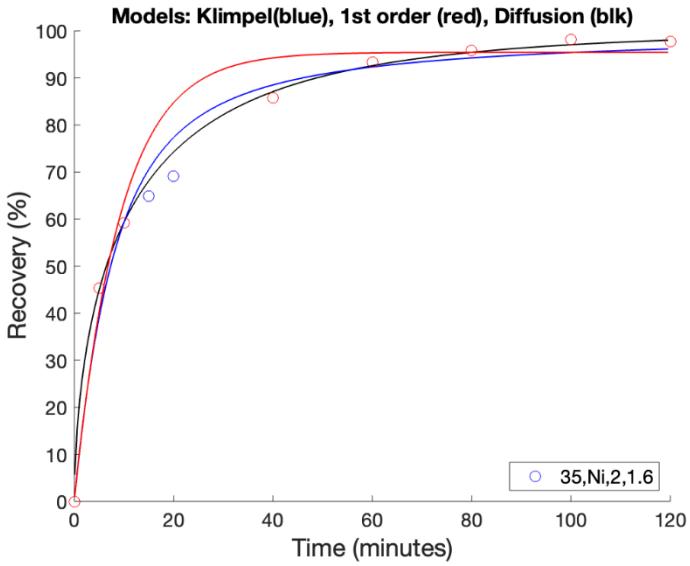

Figure 19. Kinetic models – first-order (red), Klimpel (blue), first-order diffusion-controlled (black), for Ni extraction in 2M H_2SO_4-1.6M NaCl.

To determine the correlation between the experimental and model values, the standard deviation distribution for each kinetic model was calculated using a two-tailed t-test, as shown in Figure 20. Based on the bell-shaped curve from the distribution, the standard deviation of the recovery values against the kinetic model was widely distributed in the first-order and Klimpel models while narrowly distributed in the first-order diffusion-controlled model using t-distribution. The first-order model has a mean σ of 1.15±0.38, the Klimpel model of 0.92±0.17, and the first-order diffusion-controlled model of 0.83±0.16. The σ mean values indicated that there was a tight distribution of σ around the mean value in the first-order diffusion-controlled model suggesting a more precise model compared to the other models with lower precision. Therefore, the fractional model, which was the first-order diffusion-controlled model, was a more precise model of the given leaching data.

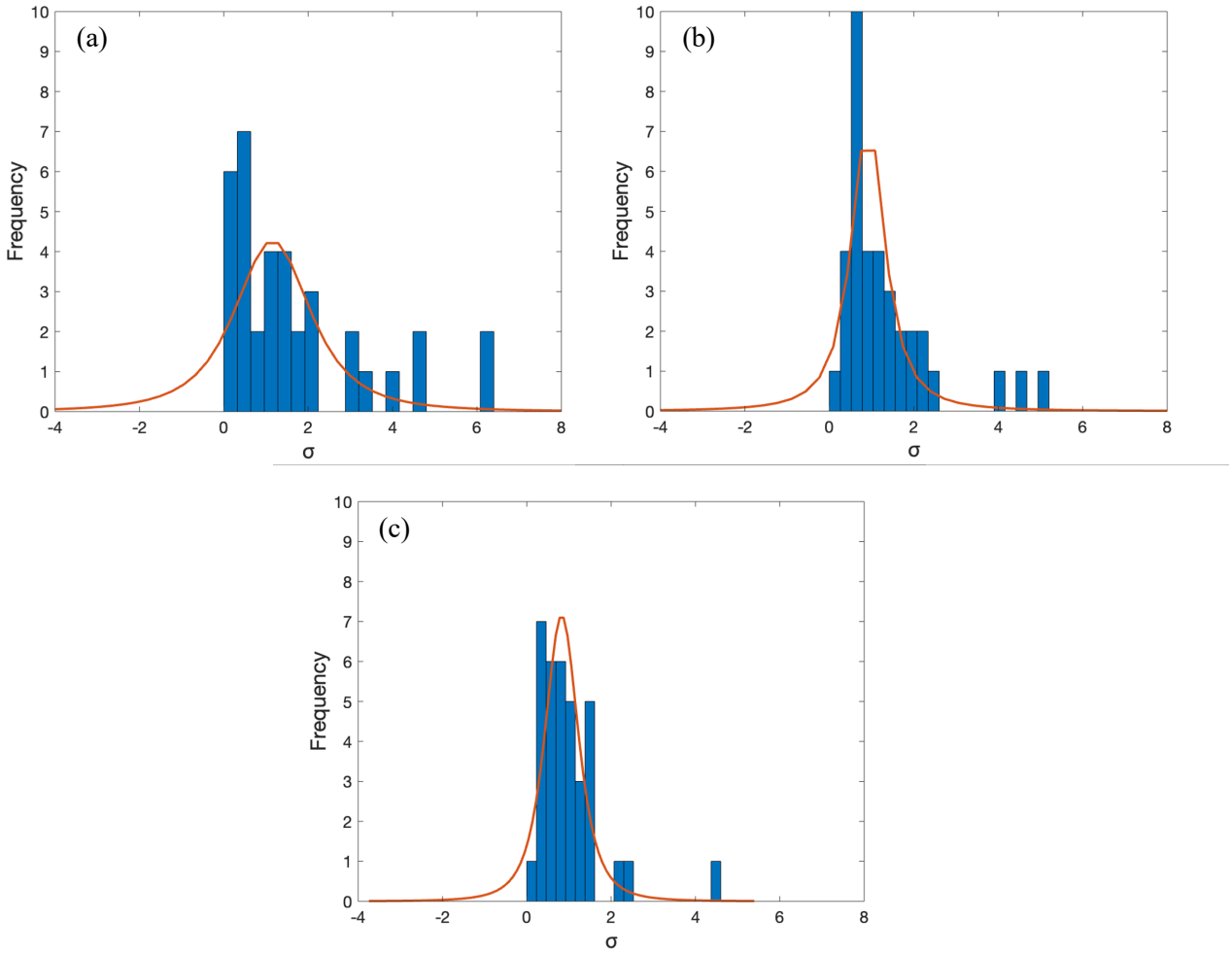

Figure 20. σ distribution in (a) first-order, (b) Klimpel, and (c) first-order diffusion-controlled kinetic model.

Since the first-order diffusion-controlled model provided the best fit, Figure 21 to 23 were parametrized with the same kinetic model at constant α for each element recovered. The maximum recovery, R_∞, was modeled in a quadratic based on the NaCl concentration for each H_2SO_4 solution in Equation 14. With the increasing NaCl concentration, k was modeled linearly with different slopes due to the difference in H_2SO_4 concentrations with the same intercepts in Equation 15. It can be seen from the figures that the addition of NaCl provided high metal recoveries of Li, Co, and Ni, especially at high acid and salt concentrations. Thus, the eight (8) different parameters that were considered in modeling the metal recoveries in this scenario were R_0, R_1, R_2, k_0, and k_1 constants in Equations 14 and 15, kinetic order α, NaCl concentration x, and H_2SO_4 concentration. The obtained parameter values to model the kinetics were shown in Table 6.

$$R_\infty = R_0 + R_1 x - R_2 x^2 \tag{14}$$

$$k = k_0 + k_1 x \quad (15)$$

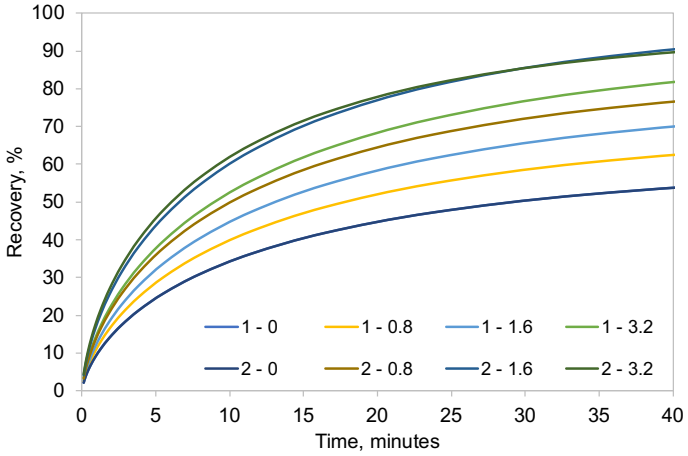

Figure 21. Li recoveries with α=0.77 (legend: H_2SO_4 concentration-NaCl concentration).

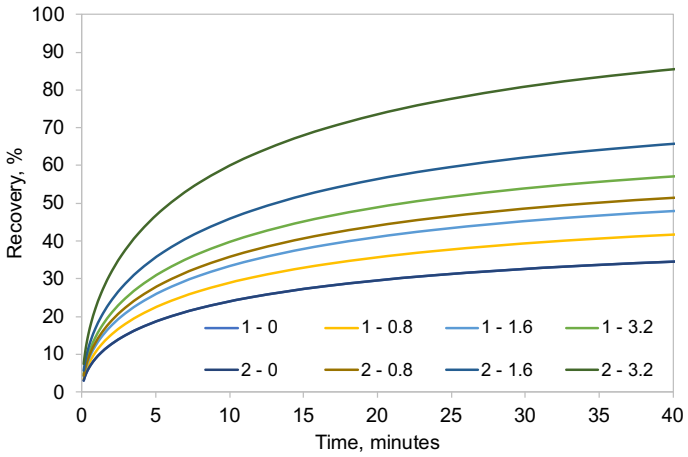

Figure 22. Co recoveries with α=0.54 (legend: H_2SO_4 concentration-NaCl concentration).

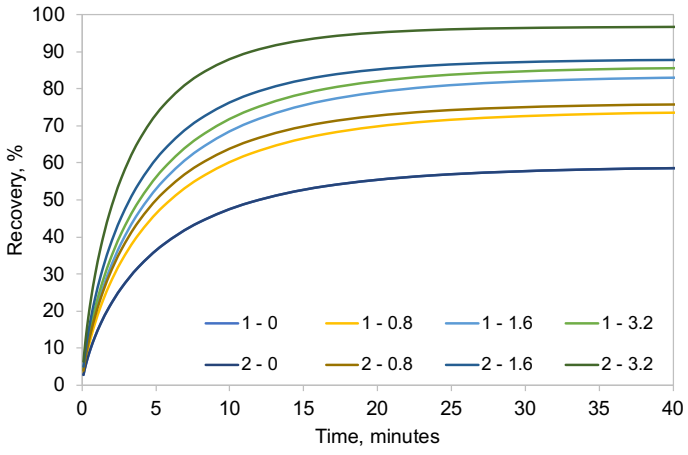

Figure 23. Ni recoveries with α=0.68 (legend: H_2SO_4 concentration-NaCl concentration).

Table 6. Values of the parameter constants to model first-order diffusion-controlled in battery leaching.

	Li	Co	Ni
α	0.77	0.54	0.68
k_0	0.27	0.26	0.17
k_1 (1M H_2SO_4)	0.009	0.001	0.001
k_1 (2M H_2SO_4)	0.041	0.003	0.013
R_0	59.09	40.77	61.49
R_1 (1M H_2SO_4)	22.30	11.49	13.00
R_2 (1M H_2SO_4)	4.34	1.00	1.00
R_1 (2M H_2SO_4)	3.94	2.71	8.13
R_2 (2M H_2SO_4)	24.39	27.19	37.08

The metal recoveries presented a fast dissociation in the first 20 minutes and slow dissociation after. This effect was relatively caused by an anomalous diffusion where the diffusivity was dependent on time. An anomalous diffusion occurs when the kinetic order α is not 1 (Simpson et al. 2013). A kinetic order $\alpha < 1$ implied that a greater amount of time was needed for the diffusants, sulfate and chloride ions, to diffuse into the material, in contrast to $\alpha > 1$ requiring less time. The α values determined from the models satisfied the conditions of an anomalous diffusion.

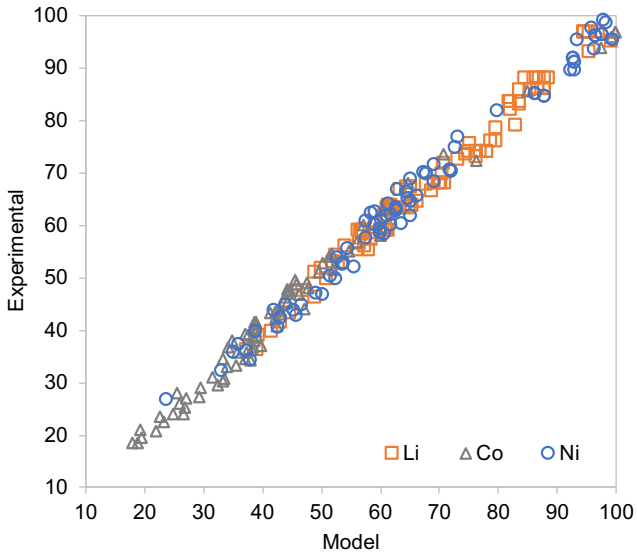

Figure 24. Regression analysis on the first-order diffusion-controlled model using 8 parameters.

A good correlation between the experimental and model recoveries was shown in Figure 24 from the regression analysis on the first-order diffusion-controlled model of the 8 parameters with R^2 of 0.9964 for Li, 0.995 for Co, and 0.9977 for Ni. The increasing α showed an increase in the favorability of metal to dissociate in the H_2SO_4-NaCl solution, conforming to the leaching kinetics from Ran et al. (2017). It can also be observed from the figures that the dissociation of Co was slow compared to Li and Ni due to the prior formation of Co_3O_4 to Co^{2+} as $CoCl_2$, further discussed in the succeeding pages. Therefore, the first-order diffusion-controlled order model can be used in leaching kinetics based on 8 parameters.

4.2 ORP measurements from different reagents

Since high recoveries were obtained from increasing concentrations of NaCl in acid leaching from the kinetic models provided, varying concentrations of NaCl solution were added to a diluted H_2SO_4 to determine the oxidizing-reducing conditions produced in the leaching solution. ORP measurements were taken using concentrations of NaCl and H_2SO_4 in grams per liter of solution to validate the results against the solution conductivities and total dissolved solids (TDS).

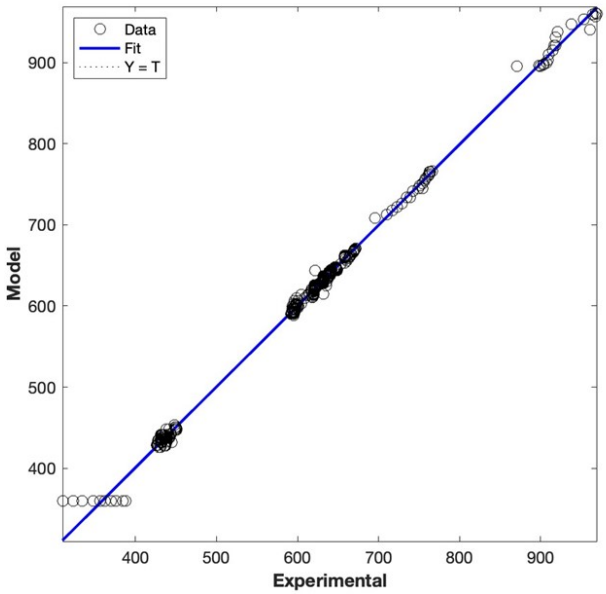

Figure 25. Regression analysis of the measured and calculated ORP.

A model was then generated to predict the ORP in NaCl-H_2SO_4 using a neural network fitting in MATLAB based on three parameters of the experimental tests – (1) temperature, (2) concentrations of NaCl and H_2SO_4, and (3) conductivities of NaCl-H_2SO_4 solutions in Appendix 3 (Robinson and Stokes 2002; Green and Perry 2008; Emerson Electric Co.

2024) against the measured ORP. In the network, the model used 80% of the data for training, 10% for validation, and 10% for testing, with the Levenberg-Marquardt backpropagation algorithm obtaining a regression of 0.9936 plotted in Figure 25. The experimental and model ORP showed a good fit from the regression, and the error distribution measured a mean error of 0.30±1.16.

An ORP model compensated in 20°C was generated in Figure 26, indicating that an increasing concentration of NaCl and H_2SO_4 increased the ORP. Different ORP values were at the same total dissolved solids due to the difference in NaCl and H_2SO_4 ratios. Since the model provided was calculated based on the six (6) concentrations of NaCl and three (3) concentrations of H_2SO_4, a complete model for ORP can be provided given with a broader range of reagent concentrations, specifically H_2SO_4, from the neural network fitting to further increase the precision of the model.

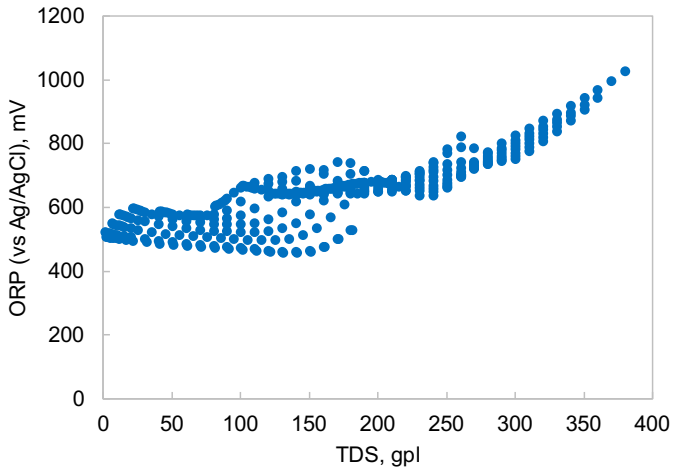

Figure 26. ORP model generated in a neural network fitting at 20°C.

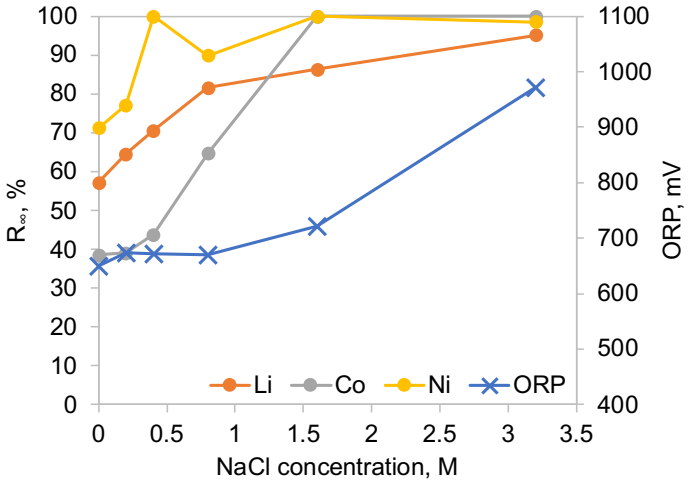

Figure 27. Maximum metal recoveries in 2M H_2SO_4-NaCl solution with calculated ORP.

From the bench-scale leaching tests of Serrano (2022), no ORP measurements were provided. However, using the model obtained from the neural network, the predicted ORP was calculated according to H_2SO_4 and NaCl concentrations. Establishing the relationship of ORP in maximum metal recoveries from the model in the addition of NaCl from Serrano (2022) recovery data, increasing the NaCl concentration of the solution showed an increase in both metal recoveries and ORP described in Figure 27. At 3.2 M NaCl addition, the ORP reached 970 mV, indicating an oxidizing condition in leaching. Thus, NaCl showed potential as an oxidizing agent in an acidic media to generate an oxidant byproduct.

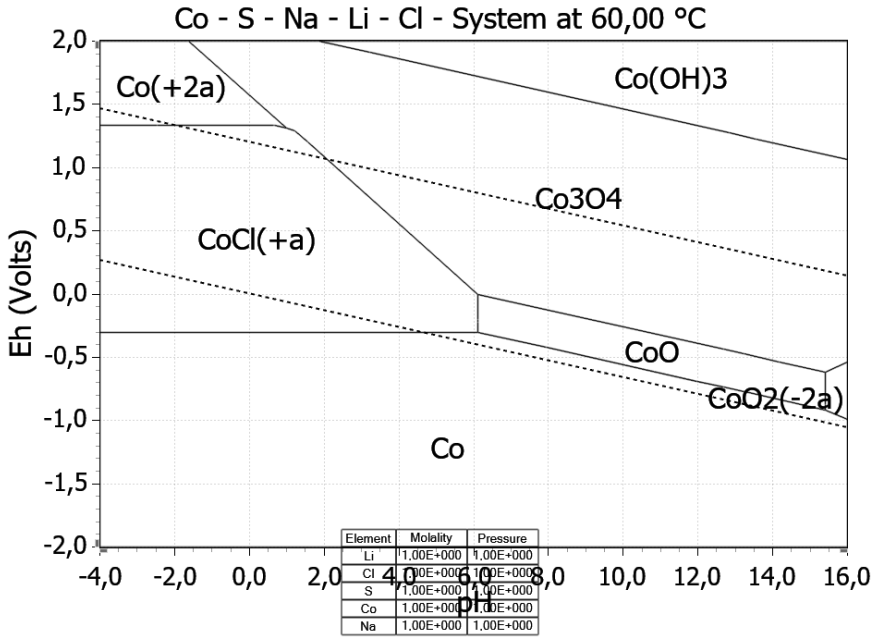

Figure 28. Eh-pH diagram of Co in H_2SO_4-NaCl system at 60°C prepared in HSC Chemistry® 10.

An oxidizing condition was generated in the NaCl-H_2SO_4 system from the high ORP measurements taken at the high NaCl concentrations. With the addition of NaCl in a sulfuric media, the Eh-pH diagram of Co shifted, shown in Figure 28, promoting the dissociation of Co^{3+} into soluble ions as described in Equation 16 at acidic and oxidizing conditions. The same goes for Ni and Li ions. This reaction was governed by the production of HCl gas shown in Equation 17 in the mixed solution of NaCl and H_2SO_4. The HCl gas was dissolved into the solution as ions to form a Cl_2 by-product described in Equations 18 and 19 increasing its oxidizing conditions (Murugappan and Silvester 2015). Cl_2 is a known strong oxidizing compound that has provided high kinetic recoveries to batch scale tests. Thus, NaCl addition in H_2SO_4 leaching generated a Cl_2 oxidant byproduct.

$$Co_3O_4 + 4H_2SO_4 + 8NaCl \rightarrow 3CoCl_2 + NaHSO_4 + Cl_{2(g)} + 4H_2O \quad (16)$$

$$2NaCl + H_2SO_4 \rightarrow NaHSO_4 + 2HCl \quad (17)$$

$$2HCl_{(g)} \leftrightarrow H^+ + HCl_2^- \quad (18)$$

$$HCl_2^- \leftrightarrow H_{(l)}^+ + Cl_2 + 2e^- \quad (19)$$

It is important to consider the stable phases of ions and compounds for leaching based in the Eh-pH diagrams. The production of oxidant byproduct, Cl_2, in the NaCl-H_2SO_4 system provided a fast diffusion kinetics of metal ions, especially with Co. For scaling-up methodologies, Cl_2 is an unwanted byproduct in the process however controllable at certain conditions in the Eh-pH diagram prepared in Figure 29. To produce metal chlorides and sulfides in the leaching process, pH should be maintained at acidic conditions of 0 to 2 and ORP between 0.50 V and 1.3 V.

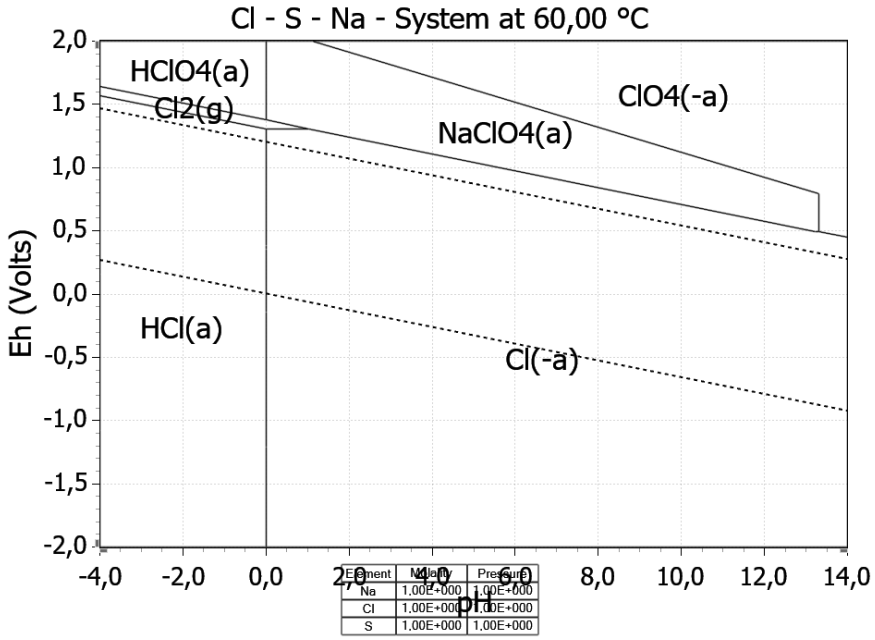

Figure 29. Eh-pH diagram of Cl in H_2SO_4-NaCl system at 60°C prepared in HSC Chemistry® 10.

Understanding the chemical dissociation of metals in the NaCl-H_2SO_4 solution has been discussed for battery leaching, however, the effect of its particle size distribution was not considered. To further improve the handling of fine sizes in the leaching of battery LMOs, results from different kinetic leaching tests for parameter optimization is discussed in the next section.

4.3 Leaching efficiency from varying parameters

Several leaching tests were conducted to determine the parameters for an efficient recovery in scale-up design and to provide more points in the kinetic modeling for fine particle leaching. Using a t-distribution for the conducted tests, the standard deviation of each kinetic model was determined. The bell curve in the σ distribution in Figure 30 was observed to be narrower in the Klimpel and first-order diffusion-controlled models than in the first-order model. To further compare the models, the mean σ values were calculated with the first-order model of 10.23±2.45, the Klimpel model of 6.85±0.81, and the first-order diffusion-controlled model of 5.44±0.59. This further concluded that the first-order diffusion-controlled model was best to describe the leaching kinetics of fine particles.

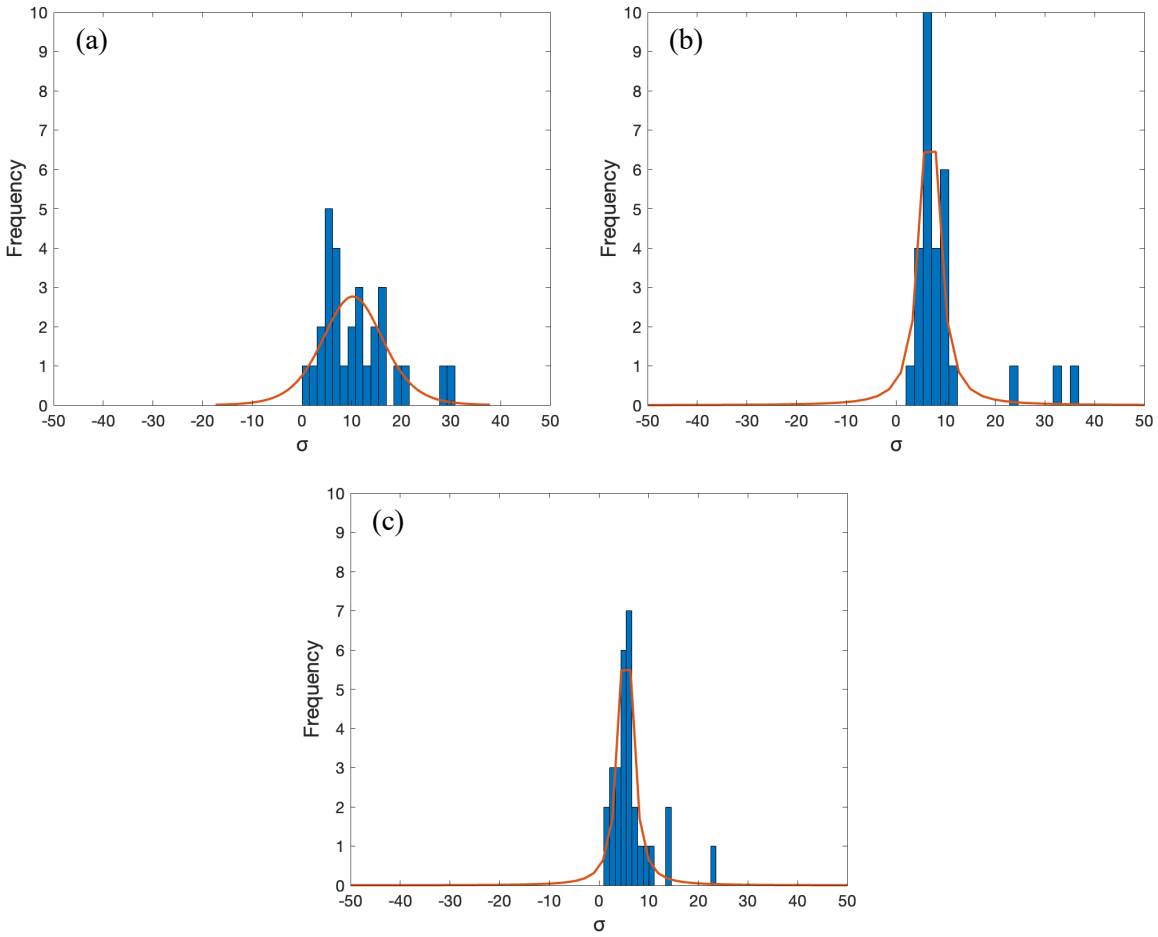

Figure 30. σ distribution of (a) first-order, (b) Klimpel, and (c) first-order diffusion-controlled models in flue dust leaching.

By increasing the temperature with 5% solids in a 250-mL solution and 0.68 m/s tip speed, an increase in Zn recovery was determined in Figure 31, which has also been concluded by the studies of Meshram et al. (2015) and Chen and Ho (2018). Using the

Arrhenius equation for the determined *k*-value in the first-order diffusion model, the activation energy was calculated as 11.18 kJ/mol. This entailed that the temperature provided an increase in the rate of reaction of the solution into the material, thus, increasing the metal recovery.

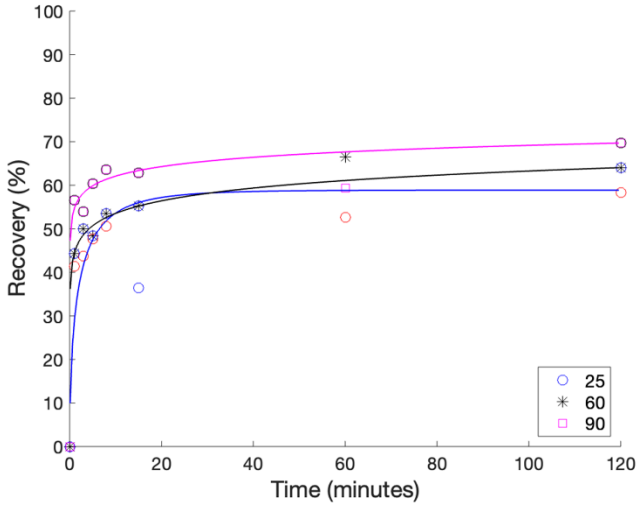

Figure 31. Zn recoveries at varying temperatures at 25, 60, and 90°C.

By varying the tip speed of the agitation at 15% solids, 0.68 m/s showed high Zn recovery as compared to 0.31 m/s and 0.94 m/s in Figure 32. Low Zn recovery was attributed to the inefficient mixing of solids in the solution of 0.31 m/s, which allowed the formation of sediments in the bottom of the beaker, and for the tip speed of 0.94 m/s, the formation of vortex maintained the suspension of the solids but also minimized the penetration of the reagent to the solid surface. The use of baffle plates was emphasized when mixing solutions at a turbulent flow to avoid vortex formation while maximizing the suspension from high agitation rates (Green and Perry 2008).

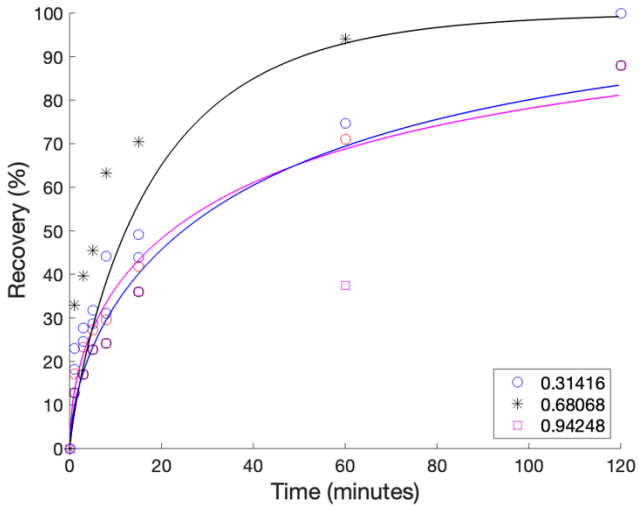

Figure 32. Zn recoveries at varying tip speeds of 0.31, 0.68, and 0.94 m/s.

To determine the optimum solid content in a reactor, varying amounts of flue dust were added in a 250-mL leaching with 0.68m/s tip speed. In Figure 33, high metal recovery was achieved at 5% and 10% solids. This indicated that lower pulp density promoted the mass transfer and dissociation of metals, increasing the leaching kinetics (Meshram et al. 2015). High pulp densities provided an increase in apparent viscosity, causing high shear stress in the reactor and decreasing the efficiency in mixing, as discussed in the literature, resulted to a decrease in Zn recovery.

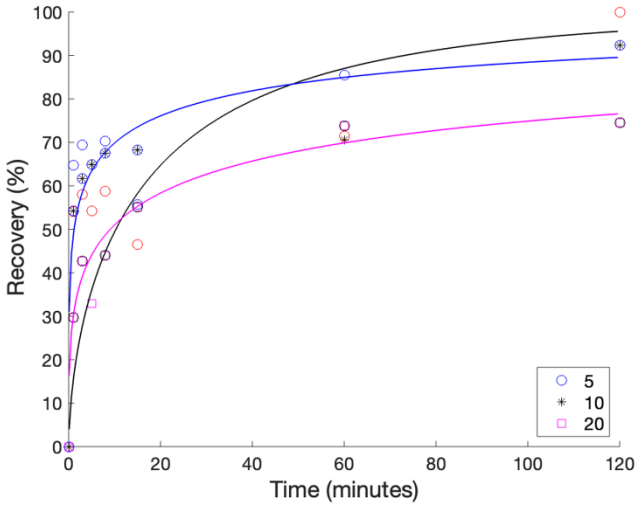

Figure 33. Zn recoveries at varying solid content of 5, 10, and 20% solids.

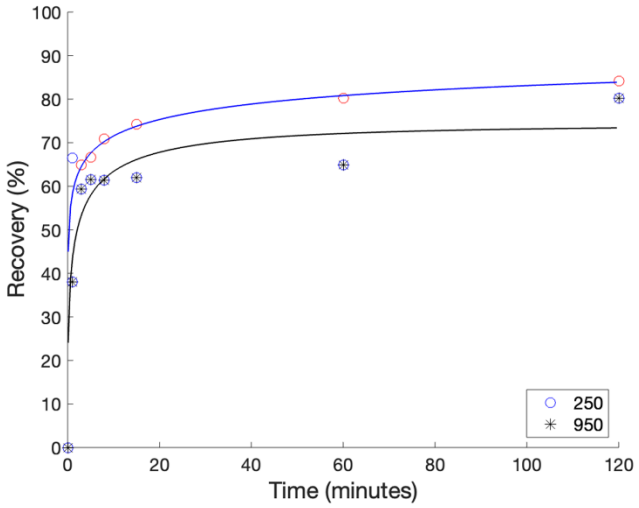

Figure 34. Zn recoveries in increased volume (in mL) with constant *Re*.

In increasing the total volume for scaling up, the Reynolds number of the agitator was maintained by retaining the same agitator features and rotational speed of 260 rpm. The recoveries of 250-mL and 950-mL solutions were shown in Figure 34. A higher recovery was observed in the 250-mL solution than in the 950-mL due to the formation of sediments at the bottom of the latter size. The diameter of the agitator was not enough to

cover the bottom of the reactor at 950 mL volume, which provided an inefficient mixing and suspension of fine particles at increased volume since the ratio of impeller and reactor diameter was not kept constant upon scaling up. Based on the impeller Reynolds number, when the diameter of the agitator was increased while the Re was kept constant, the rotational speed was decreased by a power of two increasing the apparent viscosity of the suspension because of the decrease in shear rate of the mixer. Thus, the Re cannot remain constant in scaling up due to inefficient mixing based on the test conducted.

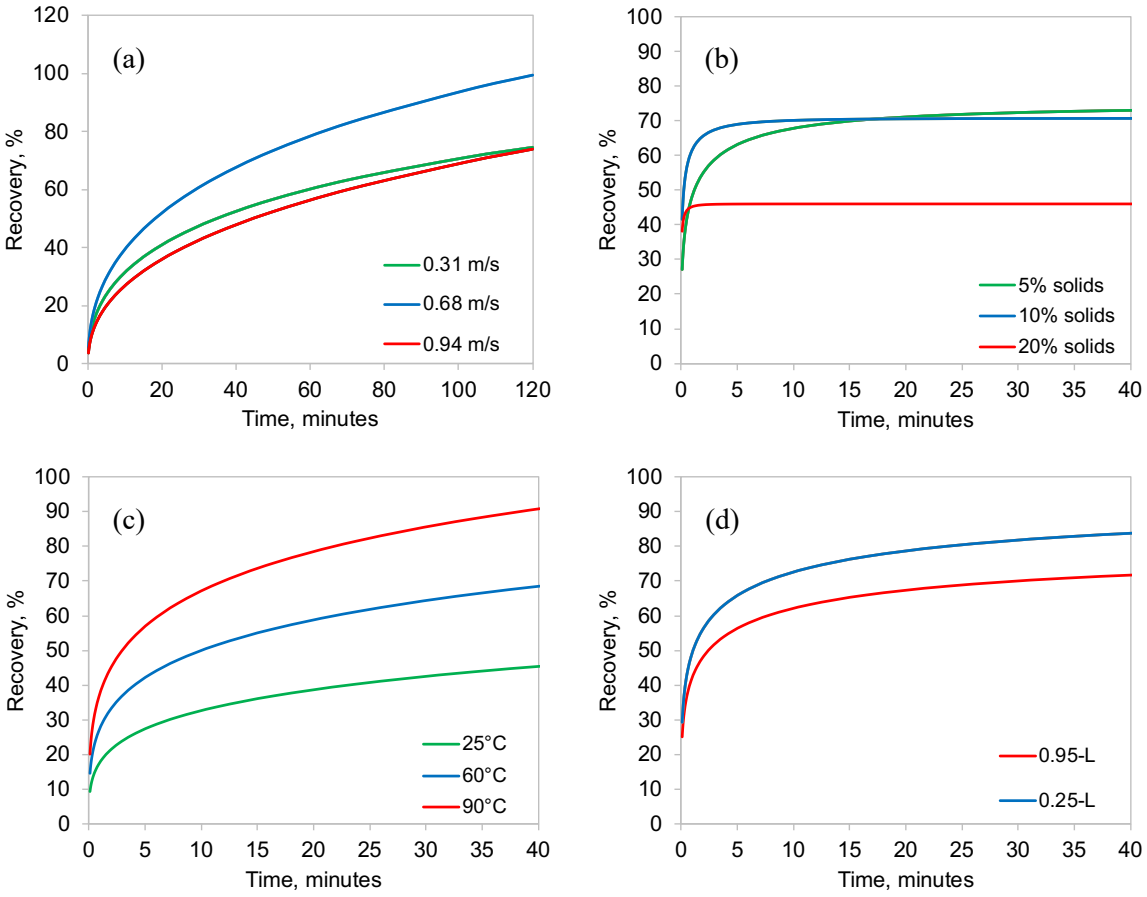

Figure 35. Recovery models for varying leaching parameters. (a) tip speed, (b) % solids, (c) temperature, and (d) volume

A similar approach was made for modeling a first-order diffusion-controlled reaction for the leaching of flue dust by parameterization. However, temperature, tip speed, solid-liquid ratio, and volume were considered as x instead of the reagent concentrations. In this case, 8 parameters were used in the model – R_0, R_1, R_2, k_0, and k_1 constants in Equations 14 and 15, kinetic order α, and leaching parameter x. The recovery models with respect to the leaching parameter were plotted in Figure 35 using the fitted constants in Table 7. The parametrized representation of the graphs provided support of the following optimal conditions of high temperature, 0.64 m/s tips speed, and at most 10%

solids. However, scaling up of volume with the same impeller conditions resulted to a decrease in efficiency.

Table 7. Values of the parameter constants to model first-order diffusion-controlled in leaching of flue dust.

Parameter constant	Temperature	Tip speed	Density	Volume
α	0.30	0.45	0.37	0.30
k_0	0.16	0.10	0.20	0.76
k_1	0.001	0.03	0.05	0.001
R_0	82.42	60.92	72.24	98.01
R_1	1.00	237.59	1.00	19.15
R_2	-	0.01	0.12	8.03

The models presented a way to design a leaching simulation, especially in handling finer sizes for battery recycling. Using the k-value from the kinetic model, appropriate selection and sizing of the reactor can be determined according to the optimal conditions identified in the kinetic tests – material flow, solid-to-liquid ratio, leaching temperature, and tip speed of the agitator. However, it must be considered that few points were measured in the model, requiring more data points to provide a more precise model and conclusions from the optimized parameters.

4.4 Battery recycling process design and simulation implemented in Aspen Plus

Considering that between 2040 and 2050, an estimated 6.6-7.5 million tons of spent lithium-ion batteries will be generated in Latin America and the Caribbean (López and Manhart 2024), with half of the volume accounted for graphite and cathode materials an estimate from a leaching plant analyzed in Aspen-Plus simulation. The application of battery recycling simulations, particularly utilizing Aspen Plus (Figure 36), has demonstrated technical and economic feasibility under certain conditions. However, further modifications to the simulation model are necessary to accurately reflect the actual kinetic data, particularly when dealing with finer particle sizes. This study aims to implement these modifications, ensuring the simulation accurately captures the leaching

kinetics and challenges associated with fine particle sizes in the recycling process of lithium-ion batteries.

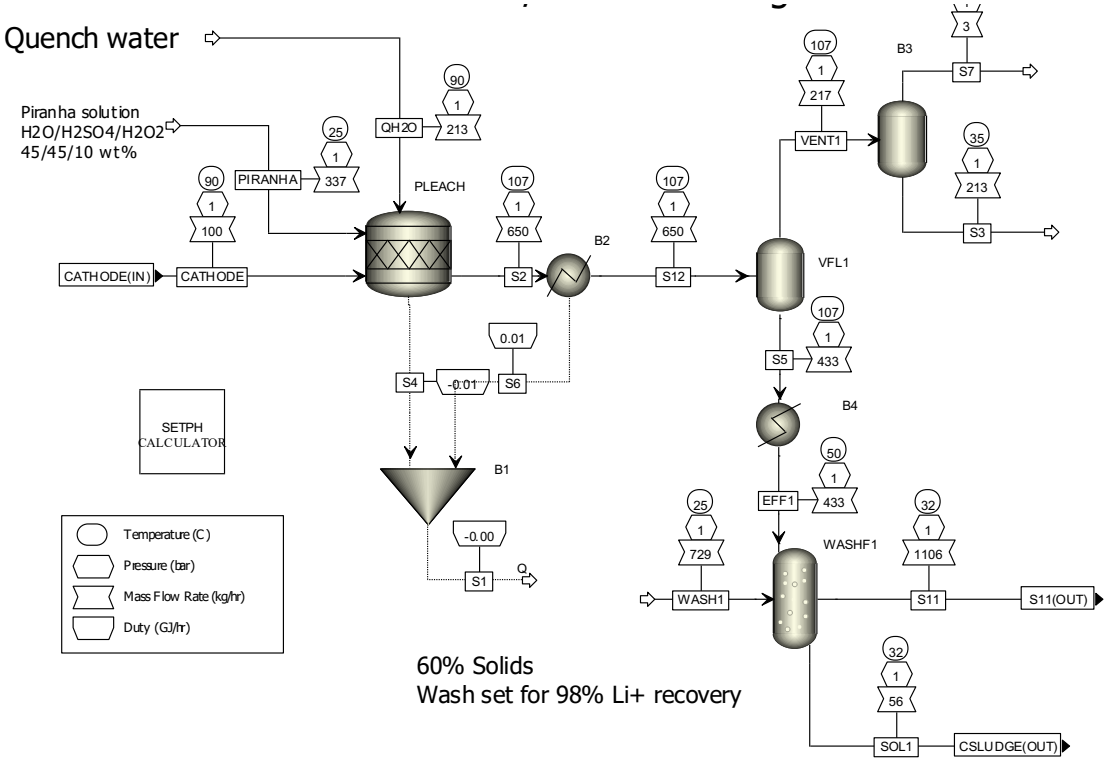

Figure 36. Aspen Plus for battery recycling simulation for H_2SO_4/H_2O_2 leaching.

Table 8. A technical-economic evaluation from Aspen Plus simulation from the initial leaching parameters in battery recycling.

Variable	Data	Unit
Total Material Cost	349	USD/hr
Total Revenue	1133	USD/hr
Total Capital Cost	10483600	USD
Annualized Capital Cost	761622	USD/year
Operating Costs	3028160	USD/year
Operational Year	8760	hr/year
Capital and Operating Cost	433	USD/hr
Total Cost	782	USD/hr
Gross Profit	352	USD/hr

Aspen Tech provided a simulation for battery recycling in Aspen Plus on the extraction of graphite and metals - Fe-Al, Cu, Co, Mn, Ni, and Li (in order of extraction) using hydrometallurgical methods – leaching, precipitation, and solvent extraction, with the general recycling flowsheet shown in Appendix 4. A piranha solution of 45wt% H_2O,

45wt% H_2SO_4, and 10wt% H_2O_2 was used in the leaching simulation added along with make-up water in Figure 36 considering that the target pH for leaching was 2. The overall recovery for the general recycling was 94.1% Cu, 94.9% Mn, 94.9% Co, 91.2% Ni, and 60.3% Li. In Table 8, a technical and economic assessment was provided from the initial simulation, considering that the process accommodates 100 kg/hr feed of material at 15% solids in atmospheric pressure and 107°C conditions. It indicated that battery recycling with the designed process and parameters was technically and economically feasible.

Focusing on the leaching stage, different scenarios in Table 9 were tested to assess the economic and technical evaluations and recoveries by applying different parameters considering Scenario 1 as the baseline of the Aspen Plus process design. Increasing or decreasing the temperature with the same feed rate did not change leaching kinetic rates and metal recoveries; however, it changed the overall recovery in Figure 37, which negatively impacted the revenue with the same expenses. The same results were attained upon changing the pressure while keeping the remaining parameters constant. By adding a fine particle size distribution obtained from the flue dust, the effect of pulp viscosity was not reflected in the overall recovery rates.

Table 9. Scenarios tested in the Aspen Plus battery recycling simulation.

	Cathode feed rate, kg/hr	Temperature, °C	Pressure, bar	with PSD	Fractional conversion
Scenario 1	100	107	1	no	1
Scenario 2	30	107	1	no	1
Scenario 3	100	107	4	no	1
Scenario 4	100	60	1	no	1
Scenario 5	100	107	1	yes	1
Scenario 6	100	107	1	no	0.8-0.9

It was assumed in the initial simulation that the metal recoveries in leaching were 100%. By varying the fraction conversion of Li, Co, and Ni extraction obtained from the bench-scale tests from battery leaching while keeping the same initial temperature, pressure, size distribution, and cathode feed rate, the solid-to-liquid ratio increased. Based on the design, the leaching reactor used was a stoichiometric reactor wherein the flow rates of feed materials were dependent on the stoichiometric reactions stored in the simulation. The % solids were calculated based on the incoming feed flow and reflected in Figure 38

with the scenarios tested. Due to the increased pulp density from applying leaching conversion of battery metals, the tendency for high shear stress in the reactor increased. The stoichiometric reactor balanced out the feed rate to the fixed product conversion while maintaining the set pH, making it unsuitable in designing battery leaching for the design provided by Aspen Plus.

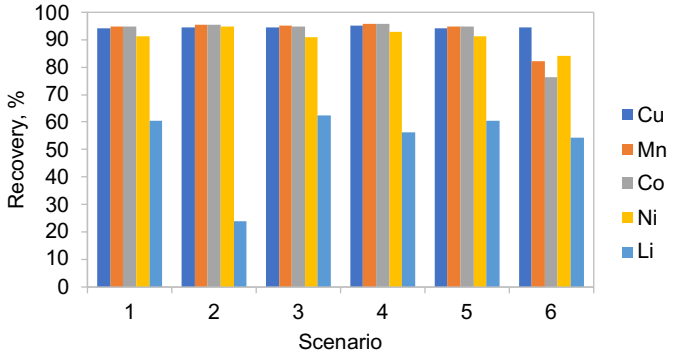

Figure 37. Metal recoveries in the overall process.

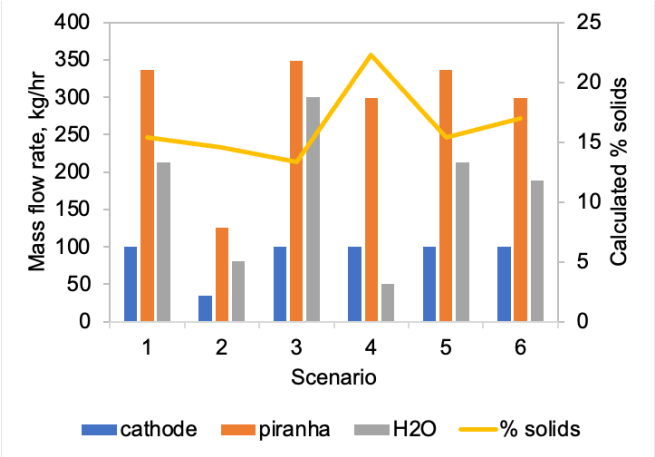

Figure 38. Mass flow rate with % solids per scenario.

The effect of changing different leaching scenarios did not significantly affect the cost analysis from the simulation, yet considerations of auxiliary equipment such as pumps were not included in the assessment. According to the cost structure from Peters et al. (2003), equipment and installation costs would describe 21% to 64% of the total capital investment. This would account for 14 to 40 million USD for the total capital cost of the design, with a gross profit ranging from 82 to 252 USD/hr, based on the total equipment and installation costs of the simulation. Despite the changes in demonstrated costing, it ensured the project remained viable under the increased capital investment. However, the reliability of this calculation is not absolute due to the exclusion of auxiliary equipment costs and potential variations in operational efficiency. Further detailed analysis and inclusion of all relevant factors are necessary to ensure a comprehensive and accurate financial assessment.

5 CONCLUSIONS AND RECOMMENDATIONS

In view of the results distinguished from different observations and tests conducted, the conclusions were as follows in line with the objectives determined.

- From the three kinetic models determined for the leaching kinetics of batteries, it was identified that the first-order diffusion-controlled model provided the lowest variances in the fitting model of residuals compared with first-order or Klimpel models. The same results for kinetic modeling were observed for the leaching test that were conducted in Zn recovery from fine particle leaching.
- The model was adjusted for a total of eight (8) parameters simultaneously for specific elements (Li, Co, and Ni) based on a first-order diffusion-controlled reaction where kinetic values are linear with the concentration of NaCl at two levels of acid concentration, while maximum recovery has a sigmoidal relationship. The α parameter was fixed for each element analyzed. Similar parameterization was achieved with Zn as kinetic values were associated with tip speed, temperature, pulp density, and reactor volume.
- A Cl_2 gas byproduct was generated from the reaction of NaCl addition in H_2SO_4 for leaching, producing an oxidizing condition to 970 mV at 143 gpl NaCl and 181 gpl of H_2SO_4. The presence of Cl_2 in the NaCl-H_2SO_4 system influenced the shift of metal ions on the Eh-pH diagram.
- The ORP of NaCl-H_2SO_4 solution can be modeled and predicted based on temperature, and NaCl and H_2SO_4 concentrations with neural network fitting.
- Fine particle leaching would reach a maximum recovery of at most 10% solids minimizing the increase of shear stress in the pulp; a tip speed of 0.68 m/s, with a 5-cm impeller diameter, ensured the suspension of fine particles and reagent penetration to the solid surface by avoiding the vortex formation from turbulent flow and sedimentation from lower tip speed; and high temperature up to 90℃ provided an increase in the rate of reaction and dissociation of metal ions into the solution.
- It was not ideal to scale up mixing reactors by maintaining similarities in Re as it can cause an increase in the apparent viscosity of the pulp and decrease the mixing efficiency.

- A stoichiometric reactor was not suitable for use in the Aspen Plus simulation for battery metal extraction because it does not account for the limitations of leaching kinetics, specifically the size distribution of the cathode material.

The following are recommended to evaluate the observations and tests conducted further.

- Improve the mixing and suspension of fine particles in solid-liquid reactors by the addition of air at increased pulp density and different mixing properties.
- Conduct more tests with a wide range of acid concentration to increase the precision of ORP model.
- Conduct leaching tests of the tails from graphite flotation, specifically from the glass-bubbles flotation with battery materials.
- Remodification of the Aspen Plus battery recycling simulation to fit the limitations leaching in handling fine-size materials, as well as the utilization of NaCl instead of H_2O_2.

6 SUMMARY

Increasing demand for Li, Co, and Ni provided shortages of supply of these materials for battery production. This opted to recycle and recover metals from spent batteries as they contain significant amounts of critical metals. However, the rheology and the presence of graphite provided difficulties in the extraction. Battery electrode materials were identified as < 15 μm, similar to the particle size distribution of flue dust from smelters. The fine size distribution of the material for leaching created high shear stress in the solid-liquid reactors reducing the reactor capacity, and the presence of graphite itself in hydrometallurgical methods increased reagent and water consumption in the leaching processes. In this context, it was aimed to evaluate the kinetics of leaching for spent batteries in varying operating parameters for scale-up methodology.

Acid leaching with the addition of chloride salt provided effective extraction from several studies. However, the leaching kinetics of the media were not evaluated, especially its oxidizing-reducing conditions. Three kinetic models – the first-order model, the Klimpel model, and the first-order diffusion-controlled model were evaluated from the bench-scale NaCl-H_2SO_4 leaching tests based on the standard deviation between the model and experimental data. It was identified that the diffusion-controlled first-order model with parameters provided a tighter distribution in the mean value σ of 0.83±0.1645 than the first-order and Klimpel models. Because of the high recoveries obtained in the tests, ORP was measured from varying reagent concentrations. The addition of NaCl in acid leaching increased the oxidation potential to 970 mV due to the generation of a Cl_2 gas byproduct. A model was then created using a neural network to predict the ORP conditions based on temperature, and NaCl and H_2SO_4 concentrations.

Since the extraction for battery cathode materials requires the leaching of fine particles, conditions at high temperatures, low pulp densities of at most 10% solids, and 0.68 m/s parameters could achieve maximum metal extraction, minimizing the shear stress in the reactors due to low apparent viscosity of the optimal conditions. However, the increase in reactor capacity by maintaining similar Re and mixer properties reduced the metal recoveries due to the inefficient suspension of fine particles. The high shear stress promoted minimized contact of the reagent and particle surface, and inefficient mixing, causing sedimentation inside the reactor, leading to low metal extraction rates. From these observations for scaling up, an evaluation of the process design provided by Aspen Plus

was conducted. Based on its technical and economic assessment of the proposed design of the battery recycling plant, it was feasible to extract the critical metals by the hydrometallurgical methods with H_2O_2-H_2SO_4 leaching. However, the consideration of fine size distribution was not accounted for in the simulation, including the leaching kinetic data, which requires further redesigning and testing.

In conclusion, the study highlights the potential of NaCl addition in H_2SO_4 leaching for extracting critical metals from spent LIBS with the importance in emphasizing optimal operating parameters to address the challenges posed by the high shear stress from fine size distribution. With this, an increased oxidation potential improved metal recoveries demonstrated kinetic recoveries in a first-order diffusion-controlled model. Despite the favorable results, further redesigning and simulations, particularly incorporating the fine particle behavior, are required for an efficient scale-up and operation of battery recycling.

REFERENCES

Aaltonen, M., Peng, C., Wilson, B. P. and Lundström, M., 2017. Leaching of Metals from Spent Lithium-Ion Batteries. *Recycling*, 2 (4), 20.

Alfaro, F., Faine, J., Jullian, R. and Gutierrez, A., 2005. Procedure to leach copper concentrates, under pressure and at ambient temperature, by forming a reactive gel in a sulfate-chloride medium. [online]. Available from: https://patents.google.com/patent/EP1559799A2/en [Accessed 23 Apr 2024].

Ali, H., Khan, H. A. and Pecht, M. G., 2021. Circular economy of Li Batteries: Technologies and trends. *Journal of Energy Storage*, 40, 102690.

Arriagada, S., Acuña, C. and Vera, M., 2020. New technology to improve the recovery of fine particles in froth flotation based on using hydrophobized glass bubbles. *Minerals Engineering*, 156, 106364.

Berg, H., 2015. *Batteries for Electric Vehicles: Materials and Electrochemistry* [online]. 1st ed. Cambridge University Press. Available from: https://www.cambridge.org/core/product/identifier/9781316090978/type/book [Accessed 1 Apr 2024].

Carneiro, M. F. C. and Leão, V. A., 2007. The role of sodium chloride on surface properties of chalcopyrite leached with ferric sulphate. *Hydrometallurgy*, 87 (3), 73–82.

Chen, W.-S. and Ho, H.-J., 2018. Recovery of Valuable Metals from Lithium-Ion Batteries NMC Cathode Waste Materials by Hydrometallurgical Methods. *Metals*, 8 (5), 321.

Chen, Y., Zhao, Z., Taskinen, P., Liang, Y., Ouyang, H., Peng, B., Jokilaakso, A., Zhou, S., Chen, T., Peng, N. and Liu, H., 2020. Characterization of Copper Smelting Flue Dusts from a Bottom-Blowing Bath Smelting Furnace and a Flash Smelting Furnace. *Metallurgical and Materials Transactions B*, 51.

Contreras, M. B. U., 2017. Evaluación Técnica y Económica de la Reutilización de Polvos de Acería para productos de Zinc en Gerdau. Universidad Técnica Federico Santa María, Valparaíso – Chile.

Dai, Q., Spangenberger, J., Ahmed, S., Gaines, L., Kelly, J. C. and Wang, M., 2019. *EverBatt: A Closed-loop Battery Recycling Cost and Environmental Impacts Model* [online]. Argonne National Laboratory (ANL), Argonne, IL (United States). No. ANL-19/16. Available from: https://www.osti.gov/biblio/1530874 [Accessed 15 Apr 2024].

Dominish, E., Florin, N. and Wakefield-Rann, R., 2021. *Reducing new mining for electric vehicle battery metals: responsible sourcing through demand reduction strategies and recycling* [online]. University of Technology Sydney: Institute for Sustainable Futures. Available from: https://earthworks.org/resources/recycle-dont-mine/ [Accessed 24 Apr 2024].

Dusing, D. C., Bishop, P. L. and Keener, T. C., 1992. Effect of Redox Potential on Leaching from Stabilized/Solidified Waste Materials. *Journal of the Air & Waste Management Association*, 42 (1), 56–62.

Emerson Electric Co., 2024. *Conductance Data For Commonly Used Chemicals* [online]. Available from: https://www.emerson.com/en-us/support/manuals-and-guides [Accessed 21 May 2024].

Ferreira, D. A., Prados, L. M. Z., Majuste, D. and Mansur, M. B., 2009. Hydrometallurgical separation of aluminium, cobalt, copper and lithium from spent Li-ion batteries. *Journal of Power Sources*, 187 (1), 238–246.

Flash Battery srl, 2022. *Lithium batteries type: which chemistry should be used?* [online]. Flash Battery. Available from: https://www.flashbattery.tech/en/types-of-lithium-batteries-which-chemistry-use/ [Accessed 6 Nov 2023].

Green, D. W. and Perry, R. H., 2008. *Perry's Chemical Engineers' Handbook, Eighth Edition* [online]. 8th ed. /. McGraw-Hill Education. Available from: https://www.accessengineeringlibrary.com/content/book/9780071422949 [Accessed 23 May 2024].

Heimes, H., Kampker, A., Offermanns, C., Klohs, D., Soldan Cattani, N., Elliger, T., Kwade, A., Ahuis, M., Michaelis, S. and Rottnick, K., 2023. *Recycling of Lithium-Ion Batteries (2nd edition, 2023)*. PEM RWTH Aachen University & VDMA.

Hernández, P. C., Dupont, J., Herreros, O. O., Jimenez, Y. P. and Torres, C. M., 2019. Accelerating Copper Leaching from Sulfide Ores in Acid-Nitrate-Chloride Media Using Agglomeration and Curing as Pretreatment. *Minerals*, 9 (4), 250.

International Energy Agency, 2021. *The Role of Critical Minerals in Clean Energy Transitions – Analysis* [online]. IEA. Available from: https://www.iea.org/reports/the-role-of-critical-minerals-in-clean-energy-transitions [Accessed 1 Apr 2024].

International Energy Agency, 2024. *The changing landscape of global emissions – CO2 Emissions in 2023 – Analysis* [online]. IEA. Available from: https://www.iea.org/reports/co2-emissions-in-2023/the-changing-landscape-of-global-emissions [Accessed 15 Apr 2024].

Jaques, A., Da Silva, C., Duru, N. and Seal, T., 2017. Fractional calculus application for diffusion controlled leaching column testing. *International Journal of Mineral Processing*, 169, 185–187.

Jung, J., Sui, P.-C. and Zhang, J., 2022. *Hydrometallurgical Recycling of Lithium-Ion Battery Materials* [online]. 1st ed. Boca Raton: CRC Press. Available from: https://www.taylorfrancis.com/books/9781003269205 [Accessed 1 Apr 2024].

Klimko, J., Oráč, D., Miškufová, A., Vonderstein, C., Dertmann, C., Sommerfeld, M., Friedrich, B. and Havlík, T., 2020. A Combined Pyro- and Hydrometallurgical Approach to Recycle Pyrolyzed Lithium-Ion Battery Black Mass Part 2: Lithium Recovery from Li Enriched Slag—Thermodynamic Study, Kinetic Study, and Dry Digestion. *Metals*, 10 (11), 1558.

Kohmuench, J. N., Mankosa, M. J., Thanasekaran, H. and Hobert, A., 2018. Improving coarse particle flotation using the HydroFloat^{TM} (raising the trunk of the elephant curve). *Minerals Engineering*, 121, 137–145.

Lin, X., Wang, X., Liu, G. and Zhang, G., 2023. *Recycling of Power Lithium-Ion Batteries: Technology, Equipment, and Policies*. Weinheim, Germany: Wiley-VCH.

Lincho, J., Gomes, J. and Martins, R. C., 2021. Paraben Compounds—Part II: An Overview of Advanced Oxidation Processes for Their Degradation. *Applied Sciences*, 11 (8), 3556.

Liu, Y., Zhang, Q. and Liu, R., 2021. Effect of particle size distribution and shear rate on relative viscosity of concentrated suspensions. *Rheologica Acta*, 60.

López, V. and Manhart, A., 2024. *Prospects for battery recycling in Latin America* [online]. oeko.de. Available from: https://www.oeko.de/en/news/press-releases/prospects-for-battery-recycling-in-latin-america/ [Accessed 4 Jun 2024].

Meshram, P., Pandey, B. D. and Mankhand, T. R., 2015. Recovery of valuable metals from cathodic active material of spent lithium ion batteries: Leaching and kinetic aspects. *Waste Management*, 45, 306–313.

Muñoz-Ribadeneira, F. and Gomberg, H., 1971. Leaching of Chalcopyrite (CuFeS2) with Sodium Chloride Sulfuric Acid Solutions: Nuclear Technology: Vol 11, No 3. *Nuclear Technology*, 11 (3), 367–371.

Murugappan, K. and Silvester, D., 2015. Electrochemical Studies of Hydrogen Chloride Gas in Several Room Temperature Ionic Liquids: Mechanism and Sensing. *Physical chemistry chemical physics : PCCP*, 18.

Navarro, P., Vargas, C., Bahamonde, F., Gómez, M., Espinoza, D., Sepúlveda, R. and Castillo, J., 2020. Effect of Pre-Treatment with Sodium Chloride/Sulfuric Acid on the Bornite Concentrate Leaching in Chloride Medium. *Metals*, 10 (12), 1674.

Neira, A., Pizarro, D., Quezada, V. and Velásquez-Yévenes, L., 2021. Pretreatment of Copper Sulphide Ores Prior to Heap Leaching: A Review. *Metals*, 11 (7), 1067.

Oosterhof, H. and Dupont, D., 2018. Process for the recovery of lithium. [online]. Available from: https://patents.google.com/patent/WO2018082961A1/en [Accessed 10 Apr 2024].

Padilla, R., Zambrano, P. and Ruiz, M. C., 2003. Leaching of sulfidized chalcopyrite with H2SO4-NaCl-O2. *Metallurgical and Materials Transactions B*, 34 (2), 153–159.

Peng, C., Hamuyuni, J., Wilson, B. P. and Lundström, M., 2018. Selective reductive leaching of cobalt and lithium from industrially crushed waste Li-ion batteries in sulfuric acid system. *Waste Management*, 76, 582–590.

Peters, M. S., Timmerhaus, K. D. and West, R. E., 2003. *Plant Design and Economics for Chemical Engineers*. McGraw-Hill Education.

Porvali, A., Aaltonen, M., Ojanen, S., Velazquez-Martinez, O., Eronen, E., Liu, F., Wilson, B. P., Serna-Guerrero, R. and Lundström, M., 2019. Mechanical and hydrometallurgical processes in HCl media for the recycling of valuable metals from Li-ion battery waste. *Resources, Conservation and Recycling*, 142, 257–266.

Prasakti, L., Yogihaz, B., Subekti, L., Sujarwo, A. and Prasetya, A., 2022. Effect of salt concentration on the properties of electrolyzed reducing water (ERW) and electrolyzed oxidizing water (EOW): an empirical correlation study. *Jurnal Rekayasa Proses*.

Quezada, V., Roca, A., Benavente, O., Cruells, M. and Melo, E., 2021. The Effects of Sulphuric Acid and Sodium Chloride Agglomeration and Curing on Chalcopyrite Leaching. *Metals*, 11 (6), 873.

Racyte, J., Rimeika, M. and Bruning, H., 2009. PH effect on decolorization of raw textile wastewater polluted with reactive dyes by advanced oxidation with U/VH2O2. *Environment Protection Engineering 35 (2009) 3*, 35.

Ran, X., Ren, Z., Gao, H., Zheng, R. and Jin, J., 2017. Kinetics of Rare Earth and Aluminum Leaching from Kaolin. *Minerals*, 7 (9), 152.

Robinson, R. A. and Stokes, R. H., 2002. *Electrolyte Solutions: Second Revised Edition*. 2nd ed. Courier Corporation.

Ruan, G., Liu, Y., Kan, A. T., Tomson, M. B. and Zhang, P., 2021. Sodium chloride (halite) mineral scale threat assessment and scale inhibitor evaluation by two common jar test based methods. *Journal of Water Process Engineering*, 43, 102241.

Serrano, C. A. A., 2022. Evaluación técnica – económica del tratamiento de baterías de ion lito (BIL) para la disolución de valores metálicos. Universidad Catolica del Norte, Antofagasta, Chile.

Sheu, S. P., Yao, C. Y., Chen, J. M. and Chiou, Y. C., 1997. Influence of the LiCoO2 particle size on the performance of lithium-ion batteries. *Journal of Power Sources*, 68 (2), 533–535.

Shimadzu Corporation, 2022. Particle Size Distribution Measurement of Lithium-Ion Battery. [online]. Available from: https://www.ssi.shimadzu.com/sites/ssi.shimadzu.com/files/pim/pim_document_file/ssi/applications/application_note/16960/PSA-2201-particle-size-of-battery-materials.pdf.

Simpson, R., Jaques, A., Nuñez, H., Ramirez, C. and Almonacid, A., 2013. Fractional Calculus as a Mathematical Tool to Improve the Modeling of Mass Transfer Phenomena in Food Processing. *Food Engineering Reviews*, 5 (1), 45–55.

Sivamohan, R. and Forssberg, E., 1985. Recovery of heavy minerals from slimes. *International Journal of Mineral Processing*, 15 (4), 297–314.

Somasundaran, P., 1980. Principles of Flocculation, Dispersion, and Selective Flocculation. *AIME*, 947–976.

Sommerville, R., Zhu, P., Rajaeifar, M. A., Heidrich, O., Goodship, V. and Kendrick, E., 2021. A qualitative assessment of lithium ion battery recycling processes. *Resources, Conservation and Recycling*, 165, 105219.

Triveni, B., Vishwanadham, B., Madhavi, T. and Venkateshwar, S., 2010. Mixing studies of non-Newtonian fluids in an anchor agitated vessel. *Chemical Engineering Research and Design*, 88 (7), 809–818.

Vanderbruggen, A., Salces, A., Ferreira, A., Rudolph, M. and Serna-Guerrero, R., 2022. Improving Separation Efficiency in End-of-Life Lithium-Ion Batteries Flotation Using Attrition Pre-Treatment. *Minerals*, 12 (1), 72.

Vinnett, L., Alvarez-Silva, M., Jaques, A., Hinojosa, F. and Yianatos, J., 2015. Batch flotation kinetics: Fractional calculus approach. *Minerals Engineering*, 77, 167–171.

Xuan, W., Otsuki, A. and Chagnes, A., 2019. Investigation of the leaching mechanism of NMC 811 (LiNi 0.8 Mn 0.1 Co 0.1 O 2) by hydrochloric acid for recycling lithium ion battery cathodes. *RSC Advances*, 2019, 38612.

Zhao, G., 2017. *Reuse and Recycling of Lithium-Ion Power Batteries* [online]. 1st ed. Wiley. Available from: https://onlinelibrary.wiley.com/doi/book/10.1002/9781119321866 [Accessed 1 Apr 2024].

Appendix 1: List of figures and tables

Table of Figures

Table of Tables

Appendix 2: External mineral and elemental characterization of flue dust

Laboratorio de Difracción y Fluorescencia de Rayos X Departamento de Cs. Geológicas

Informe Drx 025-2024

Empresa	Solicitado por
Universidad Federico Santa María	Sr. Ruvi Cobarol Marañon

Resultado composición Mineralógica Muestra Polvo de Fundición

Mineral / Compuesto	Formula Empírica	Rietveld (%)
Zincita	ZnO	61.5
Franklinita	ZnFe2O4	13.6
Cristobalita	SiO2	5.9
Vauxita	FeAl2(PO4)2(OH)2·6H2O	4.8
Manganeso	Mn	1.0
Silvita	KCl	6.1
Magnetita	Fe3O4	7.2

Difractograma General

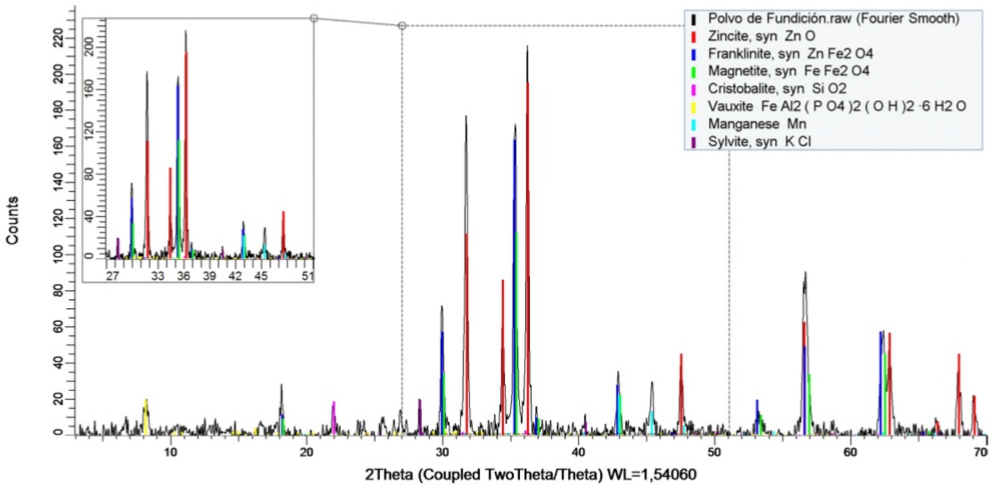

Difractograma Original

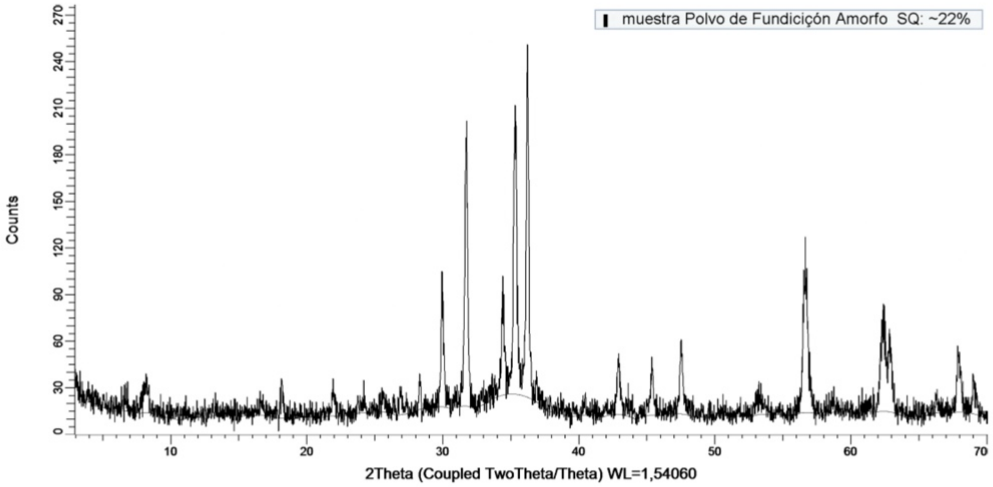

Universidad Católica del Norte
ver más allá

Informe Frx 24-2024
Fecha 25-03-2024

Señor
Sr. Ruvi Cobarol Marañon
Universidad Federico Santa María
Presente

Frx (SQ)- Muestra Polvo de Fundición

Zn	O	Fe	Cl	Pb	Ca	K	Si	Mn	S	Al	Mg	Cu	Br	Cr	Sn	P	Ba
40.90%	22.70%	21.10%	4.99%	2.34%	1.51%	1.31%	1.15%	0.92%	0.68%	0.50%	0.40%	0.33%	0.30%	0.23%	0.19%	0.11%	0.11%

Ti	Cd	Ni	V	Sr	Zr
537 PPM	479 PPM	242 PPM	130 PPM	78 PPM	57 PPM

Método Analítico: Análisis Químicos ***Semicuantitativo*** por Espectrometría de Fluorescencia de Rayos X.
Equipo: Espectrometro Secuencial de Rayos X Siemens modelo SRS3000

Atentamente

Maria Soledad Bem,bow S.
Laboratorio de Difracciòn y Fluorescencia de Rayos X
Depto. Ciencias Geológicas
Universidad Católica del Norte
Antofagasta-Chile

Appendix 3: Conductivity of the used chemicals

The conductivities of H_2SO_4 and NaCl were used in the ORP model. These data were obtained from Emerson Electric Co. (2024) and Robinson and Stokes (2002).

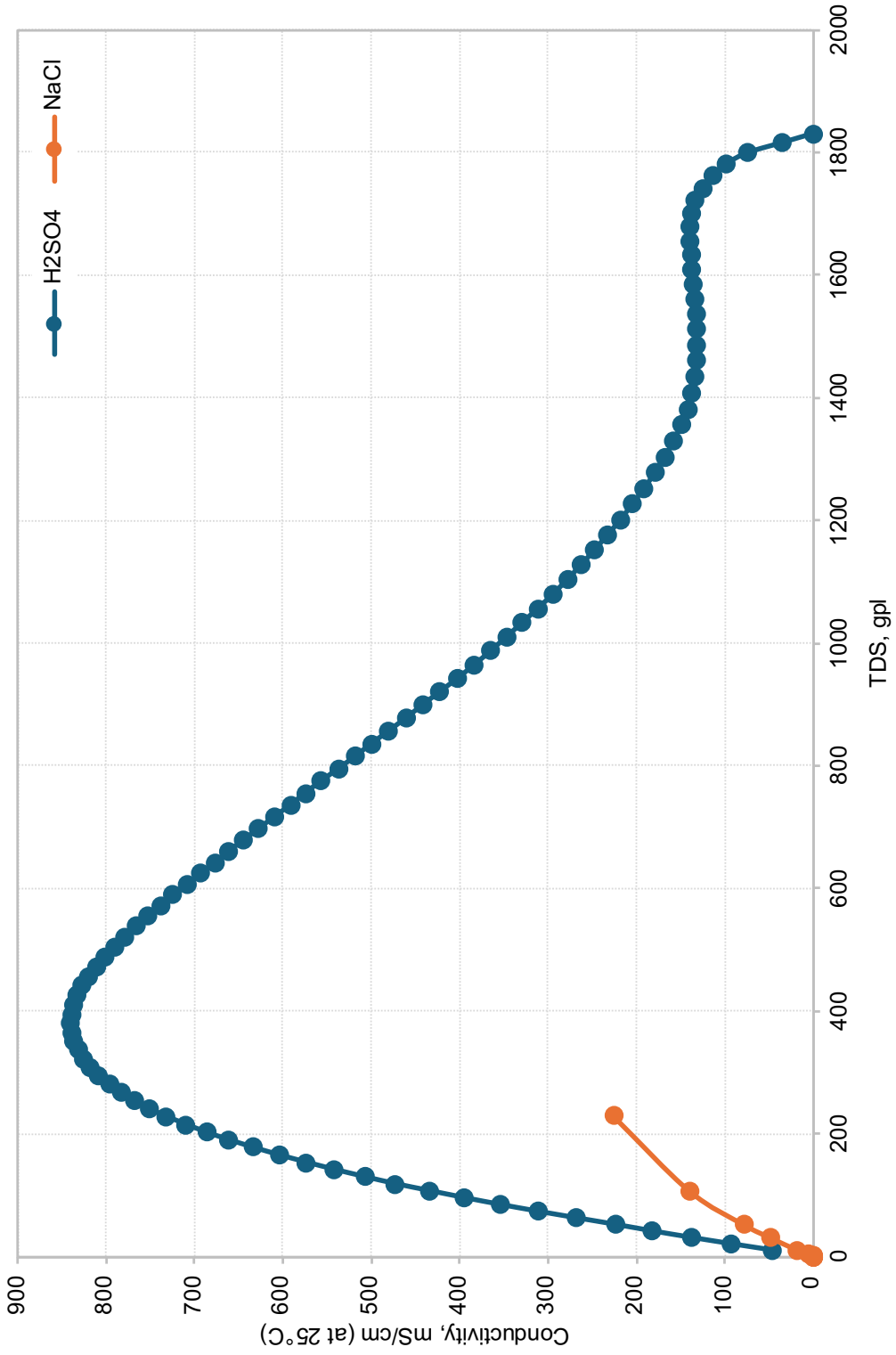

Appendix 4: Aspen Plus battery recycling main flowsheet with products